Ore Geology Reviews 104 (2019) 477–494

Contents lists available at ScienceDirect

Ore Geology Reviews

journal homepage: www.elsevier.com/locate/oregeorev

Geology, Re-Os age, S and O isotopic composition of the Lar porphyry Cu-Mo deposit, southeast Iran

Mohammad Boomeri[a,*], Rahele Moradi[a], Holly Stein[b,c], Sasan Bagheri[a]

[a] Department of Geology, Faculty of Sciences, University of Sistan and Baluchestan, Zahedan, Iran
[b] AIRIE Program, Colorado State University, USA
[c] CEED, University of Oslo, Norway

ARTICLE INFO

Keywords:
Lar porphyry Cu-Mo deposit
Sistan suture zone
Southeastern Iran
Re-Os molybdenite
$\delta^{34}S$ and $\delta^{18}O$

ABSTRACT

The Lar porphyry Cu-Mo deposit is located 20 km northeast of Zahedan in the Sistan Suture Zone (SSZ), in the southeastern part of Iran. Lar is a sub-economic porphyry Cu-Mo deposit with average grades of 0.16% Cu, 0.01% Mo, and 0.66 ppb Au. The Cu-Mo mineralization developed in post-collisional shoshonitic syenitic to monzonitic intrusions in an Oligocene igneous complex known as the Lar Igneous Complex (LIC). The host and country rocks have undergone variable degrees of supergene and hypogene alteration including silicic, potassic, propylitic, phyllic, and argillic alteration. The Cu-Mo mineralization is mainly controlled by NNW striking faults and fractures, and occurs as quartz veins and veinlets, disseminated sulfides, and stockworks. The mineralization can be divided into two types: hypogene and supergene. Hypogene mineralization is characterized by chalcopyrite, pyrite, bornite, molybdenite and magnetite, whereas supergene mineralization is characterized by enargite, covellite, chalcocite, digenite, malachite, azurite, and iron hydroxides. Sulfur isotope values for hypogene sulfides range from 0.28 to −1.76‰ and suggest an igneous source/or mantle-derived origin for sulfur. The $\delta^{18}O$ values for quartz in mineralized quartz veins range from 9.6 to 11.5‰. These values would be in equilibrium with waters having calculated $\delta^{18}O_{H2O}$ values of 9.3–11.2‰, suggesting magmatic water. Re-Os dating of two molybdenite samples from two different drill holes yields dates of 29.72 ± 0.11 and 31.95 ± 0.11, suggesting that the system was active for at least 2.0 m.y.

1. Introduction

The Lar porphyry Cu-Mo deposit is located 20 km north of Zahedan, and situated in the Lar Igneous Complex (LIC) in southeastern Iran (Fig. 1). Iran contains several distinct geological tectonic zones and provinces: (1) Zagros fold belt, (2) Sanandaj-Sirjan zone, (3) Sahand-Bazman belt, (4) Central Iran, (5) Lut and Sistan blocks, (6) Alborz zone, (7) Kopeh-Dagh zone, (8) Sistan suture zone (Flysch zone), and (9) Makran zone (Fig. 2). All zones are associated with the opening and closing of the Paleo-Tethys and Neo-Tethys oceanic basins as a result of the subduction and collision events that occurred in the northern and southern portions of Iran (Berberian and King, 1981).

The Lar porphyry Cu-Mo deposit lies in the Sistan Suture Zone (SSZ). Over the past 30 years, the SSZ and its various igneous rocks have become a key region for both petrological and tectonic studies (e.g., Camp and Griffis, 1982; Tirrul et al., 1983; Boomeri et al., 2005; Sadeghian et al., 2005; Sadeghian and Valizadeh, 2007; Rahnama-Rad et al., 2008; Ghasemi et al., 2010; Moradi et al., 2014; Mohammadi et al., 2016). However, mineralization associated with SSZ igneous rocks, such as the Lar Cu-Mo system, have been little studied (e.g., Karimi, 2002; Moradi et al., 2016). More recently, mineralization within the SSZ igneous rocks is receiving increased interest, such as the Cu mineralization in the southwestern part of the LIC. According to Boomeri (2014), the SSZ is a metallogenic province in the southeastern part of Iran that contains numerous types of mineralization including porphyry Cu-Mo, porphyry Cu-Au, Cu skarns, Sb, Au, Cu, Mn, Fe, Pb, Zn epithermal veins, Cyprus-type massive sulfides, and Alpine-type chromite. These deposits are associated with a range of rock types and tectonic environments from ophiolites to felsic igneous rocks, and flysch-type rocks in subduction, collision, and post-collisional environments. These deposits and occurrences have not yet received detailed scientific study.

The Lar porphyry Cu-Mo deposit has been explored and drilled by the National Iranian Copper Industries Co (NICICO) (Nakisa, 2002). The mineralization covers an area of 0.75 km^2, and contains several million tonnes of mineralized rocks averaging 0.16% Cu, 0.01% Mo, and

* Corresponding author.
E-mail address: boomeri@science.usb.ac.ir (M. Boomeri).

https://doi.org/10.1016/j.oregeorev.2018.11.018
Received 29 July 2017; Received in revised form 27 April 2018; Accepted 17 November 2018
Available online 20 November 2018

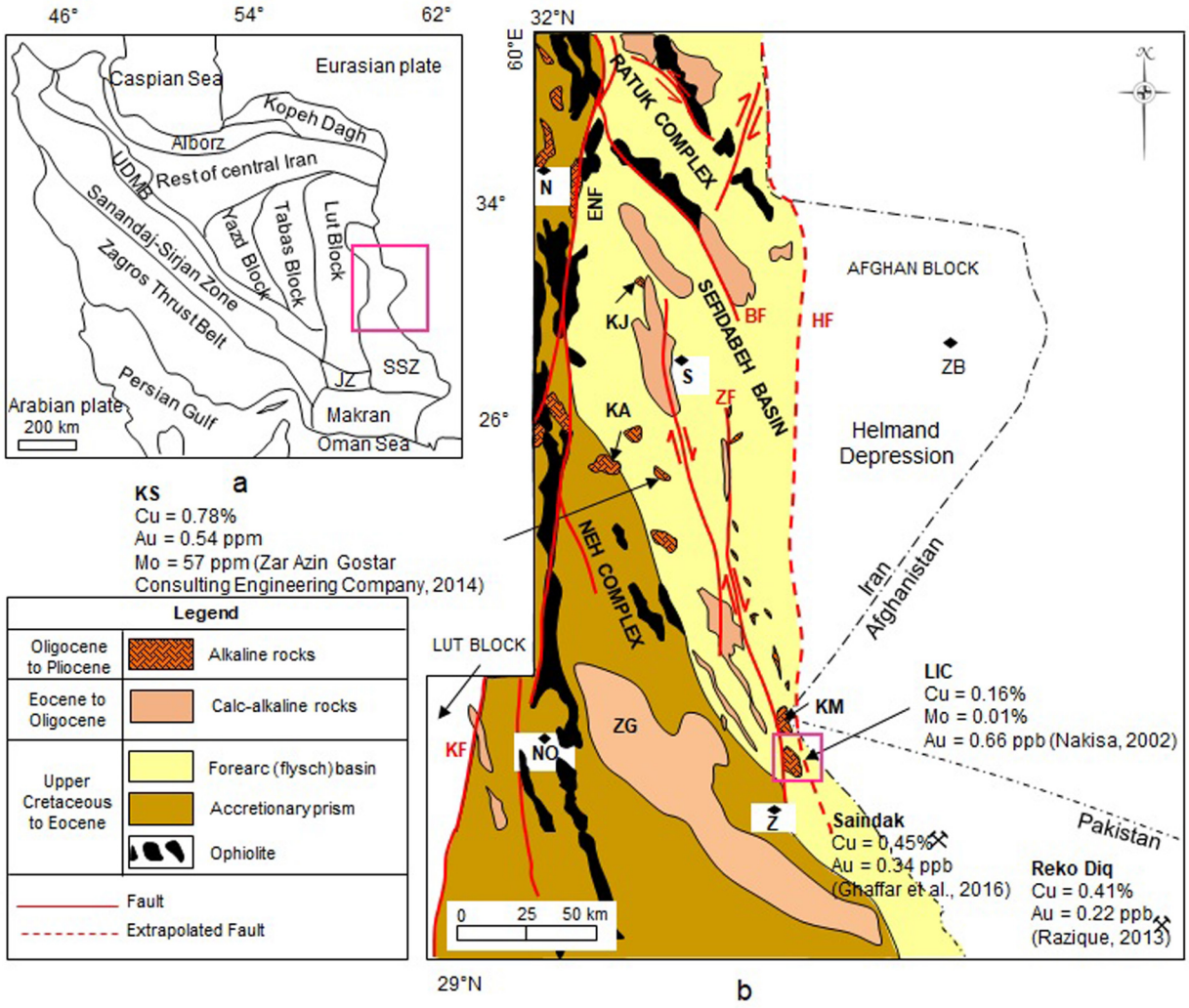

Fig. 1. Geological maps of the (a) major geological-structural zones of Iran including SSZ (Stöcklin, 1968), and (b) a part of SSZ (quadrangle in Fig. 1b) and generalized outcrop pattern of igneous rocks (modified from Camp and Griffis, 1982; Tirrul et al., 1983). UDMB: Urumieh-Dokhtar magmatic belt; JZ: Jazmorian; SSZ; Sistan suture zone; Faults are: Bandan fault (BF), East Neh fault (ENF), Zahedan fault (ZF), Kahurak Fault (KF), Harirrud Fault (HF). Place names are: Zahedan (Z), Zabol (ZB), Sefidabeh (S), Nehbandan (N), and Nosratabad (NO). Intrusions are: Zahedan granites (ZG), Lar Igneous Complex (LIC), Kuh-e Malek Siah (KM), Kuh-e Seyasteragi (KS), Kuh-e Assagie (KA), and Kuh-e Janja (KJ). (See above-mentioned references for further information.)

0.66 ppb Au (Nakisa, 2002). Although the mineralization is currently sub-economic, drilling at a nominal 250 m spacing has provided a better understanding of mineralization at depth. This study is the first paper to describe the geological, geochemical, and petrographic characteristics of the Lar porphyry Cu-Mo and its igneous host rocks. It also discusses the mineralogy, alteration, mineralization style, geotectonic environment, and possible structural controls for the Lar porphyry Cu-Mo deposit. This study also provides systematic research on Re-Os dating of molybdenite to document the timing of mineralization, and O and S isotope data to help constrain the physical and chemical condition of the fluids.

2. Regional geology

The Lar porphyry Cu-Mo deposit in the LIC is located in the SSZ (Fig. 1a). The SSZ is a remnant of a Cretaceous oceanic basin that extends as a N-S trending belt over more than 700 km along the border between Iran, Afghanistan, and Pakistan. Based on the studies of Camp and Griffis (1982) and Tirrul et al. (1983), the SSZ is characterized by the following features: (A) the presence of late Cretaceous ophiolites that are the oldest igneous rocks in this area and are the remnants of the Sistan oceanic crust between the Lut continental block to the west and the Afghan continental block to the east, (B) flysch-type rocks, the most widespread rocks in the SSZ, consisting of Cretaceous to Paleocene sedimentary, metasedimentary, and siliceous clastic rocks and (C) non-ophiolitic igneous rocks (Fig. 1b). The non-ophiolitic igneous rocks can be divided on the basis of age as follows: (1) Eocene calc-alkaline rocks of the accretionary prism that are attributed to subduction of the Lut block beneath the Afghan block (Camp and Griffis, 1982). (2) Early Oligocene Zahedan calc-alkaline I-, rare S-, and hybrid-type granitoids that are related to subduction and collision events in the area (Camp and Griffis, 1982; Sadeghian et al., 2005; Sadeghian and Valizadeh, 2007; Rahnama-Rad et al., 2008; Ghasemi et al., 2010; Moradi et al., 2014; Mohammadi et al., 2016). (3) Oligocene to Middle Miocene alkaline and calc-alkaline igneous rocks between the cities of Zahedan and Nehbandan (Camp and Griffis, 1982). The alkaline and high-K calc-alkaline (shoshonitic) magmatism is closely related to major transcurrent faults that are important post-collisional structural features (Camp and Griffis, 1982; Pang et al., 2013). (4) Quaternary volcanic rocks like Mount Taftan that are related to the Makran active subduction of the Oman oceanic lithosphere under the Makran accretionary prism and the SSZ (Farhoudi and Karig, 1977).

The SSZ was divided into the Neh-Ratuk accretionary prism and the Sefidabeh forearc basin (Camp and Griffis, 1982). The LIC is located in

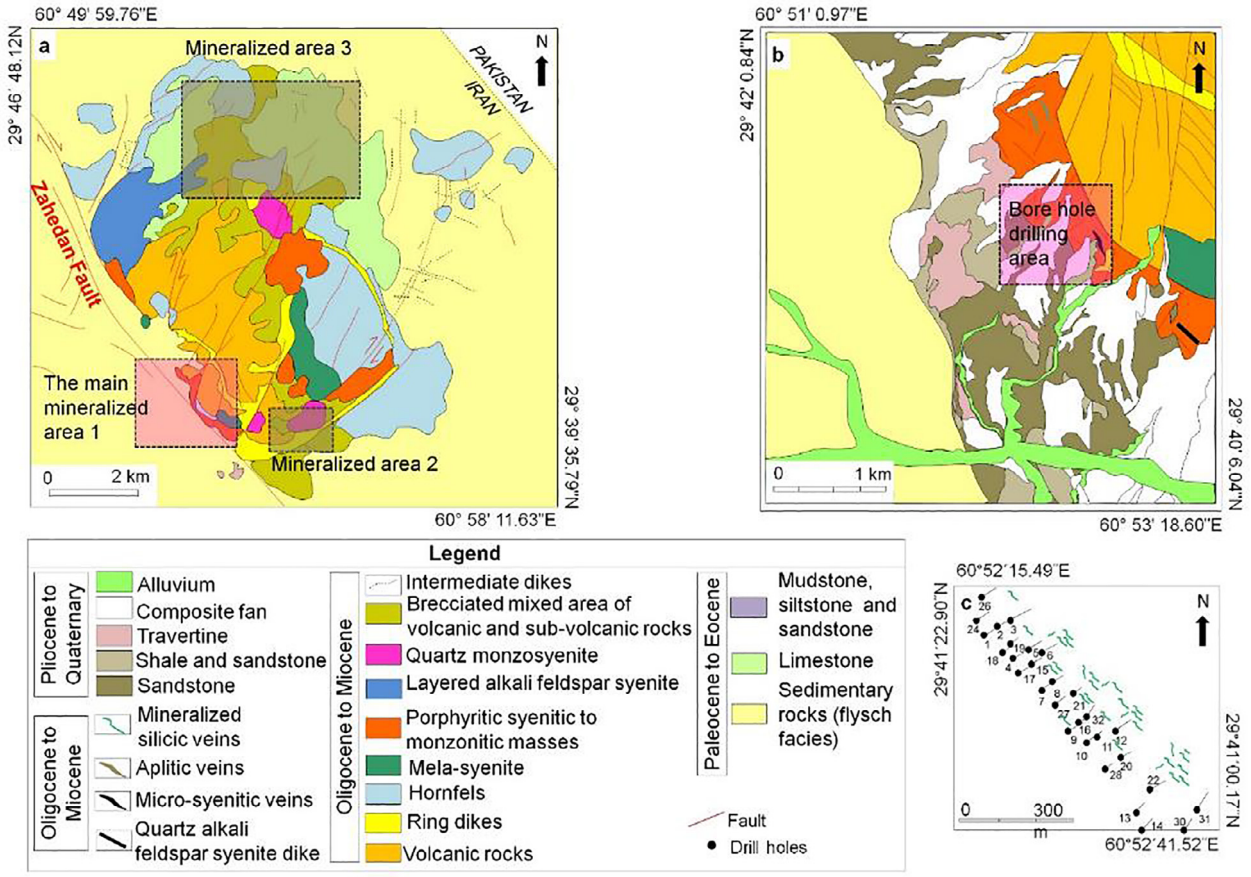

Fig. 2. (a) Geological map of the LIC including the locations that are considered as mineralized area 1, 2 and 3 (b) Geological map of the mineralized area 1 (The study area) (modified from Kan Iran engineering, 1999), and (c) bore holes locations (Kan Iran engineering, 1999) with mineralized quartz veins in the study area (The Lar porphyry Cu-Mo deposit).

the Sefidabeh forearc basin (Fig. 1b). The LIC is a late Oligocene elliptical (5 by 8 km, plan view) igneous complex that is hosted in Eocene flysch-type rocks (Figs. 1 and 2a). Its longer dimension parallels the Zahedan fault system to the west. The LIC is mainly covered by dark gray weathered lavas and pyroclastic rocks that were intruded by a polyphase intrusive stock and several dikes. Porphyry-, skarn- and vein-type mineralization is spatially and temporally associated with the magmatic activity. The volcanic rocks of the LIC are mainly porphyritic in texture, and consist of trachyte, trachyandesite, andesite, latite, latite-andesite, dacite, leucitophyre, and volcanic breccias. The LIC lamprophyric rocks include olivine minette, minette, spessartite, kersantite, and vogesite (Chance, 1981; Bagheri and Bakhshi, 2001; Ghafari-Bijar, 2009; Farokh-Nezhad, 2011). The associated magmas are alkalic, shoshonitic, and calc-alkalic in composition (Chance, 1981; Bagheri and Bakhshi, 2001; Ghafari-Bijar, 2009; Farokh-Nezhad, 2011). Plutonic and subvolcanic rocks that occur as stocks, dikes, and veins are mainly porphyritic and locally granular in texture. They consist of syenite, monzonite, quartz syenite, alkali feldspar syenite, micro-syenite, aplite, and diorite. Older igneous rocks are more mafic, whereas younger ones are progressively more felsic (Camp and Griffis, 1982).

Structurally, the SSZ is an active zone of N-S right-lateral strike-slip faulting that roughly defines the eastern border of Iran. The Zahedan, east Neh (west Assagie), and west Neh faults are active structures in the SSZ (Walker and Jackson, 2004) (Fig. 1b). The Zahedan fault is the easternmost of the active faults and is almost 150 km long. At its northern end, the Zahedan fault ends at the Sefidabeh blind thrust (Walker and Jackson, 2004) (Fig. 1b). The east and west Neh faults are two subparallel faults, each with a length of almost 200 km. To the south, they end near Nosratabad and the Neh faults appear to link southward with the Kahurak and Nosratabad faults (Fig. 1b).

3. Geology of the mineralized area

The main outcrop of the Lar porphyry Cu-Mo deposit is situated in the western and southwestern part of the Lar igneous complex (LIC) which consists of various flysch units, and igneous rocks with some recent surficial deposits (Fig. 2b). The Lar igneous rocks are hosted by Upper Cretaceous, Paleocene, and Eocene flysch-type rocks, such as siliceous shale, sandstone, siltstone, and minor limestone (Fig. 2a). The flysch rocks are the oldest units in the Lar area and are also predominant in the SSZ. They are locally altered and metamorphosed around the LIC. At the contact with the LIC intrusion, shales are metamorphosed to fine-grained, siliceous biotite-epidote hornfels. The hornfels units are prominent around the eastern edge of the mineralized area and in the center and along the southern margin of the LIC. Based on microscopic studies, the hornfels are characterized by the assemblage quartz, K-feldspar, biotite, sericite, epidote, and chlorite. Results from drilling suggest some parts of the hornfels are enclaves in the intrusive rocks. Shale that crops out in the western part of the mineralized area is red, yellow, and brown, indicating oxidation of pyrite and/or supergene alteration. Fig. 2c shows the location of boreholes in the mineralized area.

Field photographs of the western and southern parts of the LIC, including the mineralized zones, are shown in Fig. 3a–g. Igneous rocks in the mineralized area include extrusive volcanic rocks and intrusions. The extrusive rocks include both lavas and tuffs that overlie flysch-type rocks. The highest elevations in the LIC are underlain by lavas whereas low, recessive areas tend to be underlain by pyroclastic rocks. The

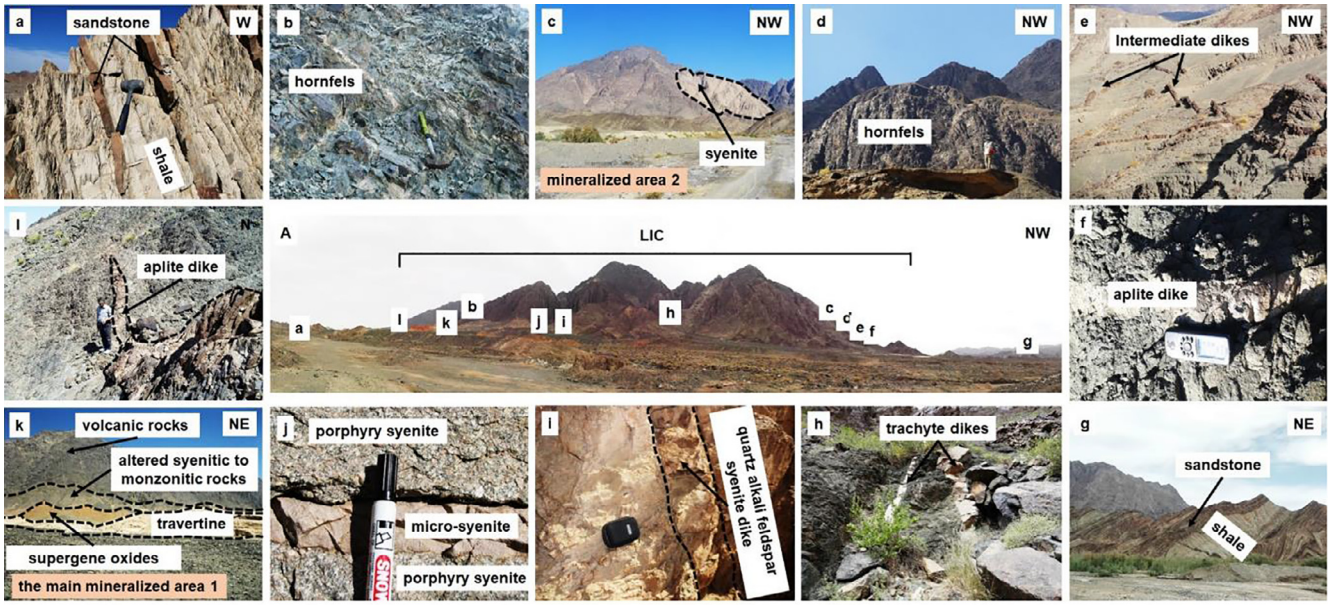

Fig. 3. Field photographs of the LIC and the lithological units (A) view of the LIC from southern and western parts, the characters are parts that are enlarged in other photographs shown in this figure (a) steeply dipping interlayered shale and sandstone with subvertical refracting cleavage of the host of the LIC, (b) hornfels in the southwestern part of the LIC, (c) porphyritic syenite in the southeastern part of the LIC, (d) subvertical hornfels in the eastern part of the LIC, (e) intermediate dikes in the eastern part of the LIC, (f) aplite dikes in the eastern part of the LIC, (g) interlayered shale and sandstone in the eastern part of the LIC, (h) trachyte dikes that cutting subvolcanic units in the southwestern part of the LIC, (i) quartz alkali feldspar syenite dike cutting syenite unit in the southwestern part of the LIC, (j) micro-syenite dike cutting porphyry syenite in the southwestern part of the LIC, (k) travertine in southwestern part of the LIC, and (l) aplite dike in southwestern part of the LIC.

Fig. 4. NE-SW fault that cuts the mineralized area and the LIC.

intrusives occur as stocks and dikes. The intrusive stocks are mainly pink to gray, porphyritic and equigranular syenite and monzonite. These rocks are cut by mineralized and unmineralized quartz veins and veinlets. Furthermore, the stocks are intruded by some aplitic and very fine-grained syenitic dikes and veins. The syenitic and aplitic dikes and veins are texturally distinct from the host syenite to monzonite intrusions. Igneous rocks in the mineralized area are similar to unmineralized rocks elsewhere in the LIC. There are at least two fault and fracture systems in the mineralized area. The oldest is the main fault system with a NW-SE strike, along which the mineralization is focused. The youngest fault system strikes NE-SW and clearly cross-cuts all mineralization and the LIC (Fig. 4).

4. Methods

Geological maps of the LIC and the main Cu-Mo mineralized area in the southwestern part of the LIC were prepared based on satellite images and field and laboratory studies (Moradi, 2016). A total of 200 samples were collected from the mineralized syenitic to monzonitic intrusions, mineralized quartz veins, and barren quartz veins. Standard polished thin sections were made. Thin sections were examined using a polarized microscope for petrographic and mineralogic descriptions at University of Sistan and Baluchestan in Iran. Major and trace element analyses were obtained from 18 samples of the Lar host igneous rocks (Table 1). Major and trace elements were determined by $LiBO_2$ fusion and measured by XRF techniques, and some trace and rare earth elements were obtained by $LiBO_2$ fusion and measured by ICP-MS techniques at ACTLABS laboratory in Canada.

Oxygen isotope studies were carried out on the following samples: whole rocks from the syenitic to monzonitic host intrusions; rocks from the potassic, phyllic, propylitic, and argillic alteration zones (8 samples); and pure quartz from the mineralized quartz veins and veinlets (3 samples). Sulfur isotope studies were carried out on separates of chalcopyrite, bornite, and molybdenite. The mineral separates were purified by crushing and hand-picking to a purity of ~99%. The isotopic compositions of oxygen were determined in the ACTLABS laboratory in Canada. Oxygen was extracted from powders using the ClF3 method of Borthwick and Harmon (1982), and quantitatively converted to CO_2 over red-hot graphite. Oxygen-isotope measurements were performed using an Optima dual-inlet stable isotope ratio mass spectrometer. Oxygen-isotope results are presented in the normal delta-notation relative to VSMOW using a two-point calibration curve based on internal standards. Using this calibration curve, average values of 9.65 and 5.2‰ were obtained for NBS-28 and NBS-30, respectively, which compare well with their accepted values of 9.57 and 5.12‰, respectively. The precision of duplicate analyses of unknown materials was normally better than ± 0.2‰, as determined from duplicate analyses of representative samples.

The sulfur isotope analyses were performed using the EA-IRMS technique at the Iso-Analytical laboratory of London. Isotopic analyses were performed on SO_2 gases extracted by conventional methods (Ohmoto and Rye, 1979; Ohmoto and Goldhaber, 1997) from the

Table 1
Representative major oxide (wt%) and trace elements (ppm) analyses of igneous host rocks from the Lar porphyry Cu-Mo deposit.

Sample	RM1	Rbef.2	RIM	RM4	RM5	RM6	RIA7	RMS	RM9	RIA10	Ma11	RI12	RI13	RIA14	RIA15	RI16	RE117	RE118
SiO_2	58.45	57.14	58.3	62.2	58.8	58.3	58.1	64.2	61.6	59.7	67.7	61.2	61.69	57.39	58.52	56.15	59.22	61.24
Al_2O_3	17.31	17.42	172	17.4	17.3	18.2	18i	14.9	17.7	17.5	14.8	16.46	15.07	16.54	16.28	11.44	13.93	13.03
Fe_2O_3	5.33	4.14	5.55	3.42	5.94	3.94	4.2.8	3.95	3 J	3.59	1.39	4.23	3.92	4.27	4.21	1.11	3.63	4.21
MnO	0.08	0.08	0.05	0.04	0.08	0.04	0.08	0.02	0.04	0.03	0.01	0.07	0.04	0.03	0.04	0.02	0.04	0.04
MgO	2.78	1.8	2.39	1.17	0_31	2.11	2.19	0.67	0.24	2.11	0.11	1.17	2.34	0.13	1.62	2.1	1.61	1.81
CaO	3.42	2.61	3.87	228	1.4	2.43	161	0.48	1.2.4	1.33	0.53	2.9	2.69	1.23	3.12	2.19	221	174
Na_20	4.78	4.2.	4.82.	4.83	4.67	5.05	431	3.11	4.15	533	2.34	5.01	3.1	3.52	4.51	4.73	3.92	5.08
IC.0	5.37	6.04	5.17	7.37	7.05	6.2.7	7.34	7.68	8.13	6.17	8.58	6.05	3.01	3.71	8.55	9.43	8.05	6.02.
TiO_2	0.6	0.47	0.51	0.35	0.68	0.49	0.47	0.2.4	0.57	0.43	0.33	0.47	0.44	0.55	0.74		0.43	0.41
F.A.	0.69	0.56	0.6	0.38	0.38	0.6	0.56	0.2.7	0.66	0.53	0.32.	0.39	0.51	0.56	0.71	0.98	0.52.	0.46
LOI	1.72	1.7	0.83	0.88	3.02.	2.6	1.7	1.39	1.94	1.95	1.84	2.11	2.91	2.3	1.66	1.9	1.33	0.79
Total	100.6	96.16	100.1	100.7	100.5	100	100.1	97.31	99.37	98.67	97.95	100.5	99.32	94.63	99.96	98.05	98.93	99.87
Zr	192	117	197	115	190	180	120	118	191	132	119	218	147	29	36	85	112	211
Co	13	11	113	10.1	12.4	11.5	11.4	8.2	8.9	103	1.4	9	11	5.9	8.2	10.2	9	9
Cu	90	670	1123	556	2132	1662	673	13,333	4337	13,333	13,333	70	3600	14,105	197	9934	1660	430
Nb	14	14	19	17	22	19	20	9	15	13	20	12	8	16.1	172	14.6	10	13
Th.	21.6	12	15.9	18.2	21.4	16.4	116	8_6	133	15.3	22.4	192	173	1/6	243	143	14.1	25.3
Mo	< 2.	62	47	56	30	19	65	308	50	15	50	4	91	210.6	16	13.1	34	4
La	32.9	31	26.9	22.5	28	30.4	30.6	9.6	24.6	36.7	19.9	31.4	22	16	28	39	25.5	29.5
Ce	57.8	50	47.4	40.5	49.2	49.8	501	17.2	43.2	51.6	32.6	55	40.5	31	47	59	42.1	49.7
Hf	3.8	4	5	7	5	4	4	2	5	4	4	4.5	2.8	1.11	1.24	1.43	2	4.4

sulfur-bearing minerals. Sulfur isotope values were measured against the standard VCDT, and reported as $\delta^{34}S$ (‰) notation with an overall analytical reproducibility of ± 0.1‰. The reference material used for sulfur isotope analysis was IA-R061 (barium sulfate, $\delta^{34}S_{V\text{-}CDT}$ = 20.3‰). For each sample, approximately 5 mg of sulfide separates was weighed into tin capsules and combusted with an elemental analyzer connected to a continuous flow isotope ratio mass spectrometer.

For the Re-Os dating of molybdenite, mineral separates were obtained using a small hand drill and were 100% pure molybdenite. A weighed amount of molybdenite powder was equilibrated with a mixed-double Os spike (Markey et al., 2003), using a Carius tube dissolution vessel. Re and Os isotopic ratios were measured by NTIMS (negative thermal ionization mass spectrometry) on a Triton machine at the AIRIE Program, Colorado State University. All reported data are blank corrected and at two-sigma uncertainty.

5. Petrography

Based on field and petrographic studies, the igneous rock units in the LIC can be divided into extrusive and intrusive rocks.

5.1. Extrusive rocks

The extrusive rocks comprise lavas and tuffs. Compositionally they include porphyritic trachytes, latites, and andesites, pyroclastics, and lamprophyres (Fig. 5). The phenocrysts are sanidine, plagioclase, clinopyroxene, hornblende, biotite, quartz, and opaque minerals that constitute 50% of the rock volume. The groundmass is composed of very fine-grained feldspar with minor ferro-magnesian minerals. Plagioclase and sanidine phenocrysts are variable in size (up to 5 mm) and shape. The feldspars in the extrusive rocks are partially altered to chlorite, epidote, calcite, sericite, and kaolinite. Clinopyroxene is an abundant mineral in the lamprophyric rocks where it may form up to 50% of the rock by volume.

5.2. Intrusive rocks

Based on the modal classification, the intrusive rocks in the mineralized stock include syenite, monzonite, quartz syenite, and alkali feldspar syenite. The intrusives are mainly equigranular and porphyritic in texture. These rocks mainly contain mineralized quartz veins and veinlets that locally form quartz stockworks.

5.2.1. Syenite and monzonite

The syenite and monzonite group of rocks are dominantly porphyritic, and contain mainly K-feldspar, plagioclase, clinopyroxene, amphibole, and biotite. Accessory minerals include titanite, apatite and zircon. The K-feldspar is mainly perthitic and poikilitic in texture, subhedral to euhedral, and variable size (up to ~3 cm) (Fig. 6a and b); it is partially replaced by kaolinite. Plagioclase is tabular to lath-shaped, with oscillatory zoning, polysynthetic twining, and a variable size (up to 2 mm); it is partially replaced by sericite. Primary biotite is subhedral to euhedral, variable in size, light to dark brown in color, strongly pleochroic (Fig. 6c), and locally altered to chlorite. Some biotite that is finer-grained and lighter in color forms around and inside of clinopyroxene, amphibole and opaque minerals, and also occurs in fractures. Clinopyroxene and amphibole occur as euhedral to subhedral crystals (Fig. 6d) that are partially to totally replaced by chlorite, epidote, calcite, and biotite. The groundmass of the porphyritic rocks also contains K-feldspar, plagioclase, biotite, muscovite, aegirine, microcline perthite, and calcite. The most common alteration minerals are chlorite and sericite.

5.2.2. Quartz syenite

The quartz syenite rocks contain K-feldspar, plagioclase, and quartz as the main minerals, and clinopyroxene, amphibole, and biotite as mafic minerals. The accessory minerals are titanite, opaque minerals, apatite, and zircon. The tabular and euhedral to subhedral crystals of K-feldspar are mainly orthoclase, but microcline is also present. Some of the phenocrysts of K-feldspar contain poikilitic inclusions of plagioclase, biotite, titanite, and opaque minerals. The plagioclase is euhedral to subhedral, and it encloses biotite, apatite, and opaque minerals. The quartz appears as a late mineral phase and fills interstices between other minerals. Quartz is intergrown with both plagioclase and K-feldspar, and occurs as veinlets related to the hydrothermal system (Fig. 6e). The most common alteration minerals are chlorite and sericite.

5.2.3. Alkali feldspar syenite dikes, and other dikes and dikelets

Alkali feldspar syenite occurs as medium-grained equigranular dikes (Fig. 6f) that mainly contain K-feldspar and small quantities of plagioclase, amphibole, clinopyroxene, and biotite. The K-feldspar and local microcline constitutes up to 90% of the rock by volume. The dikes

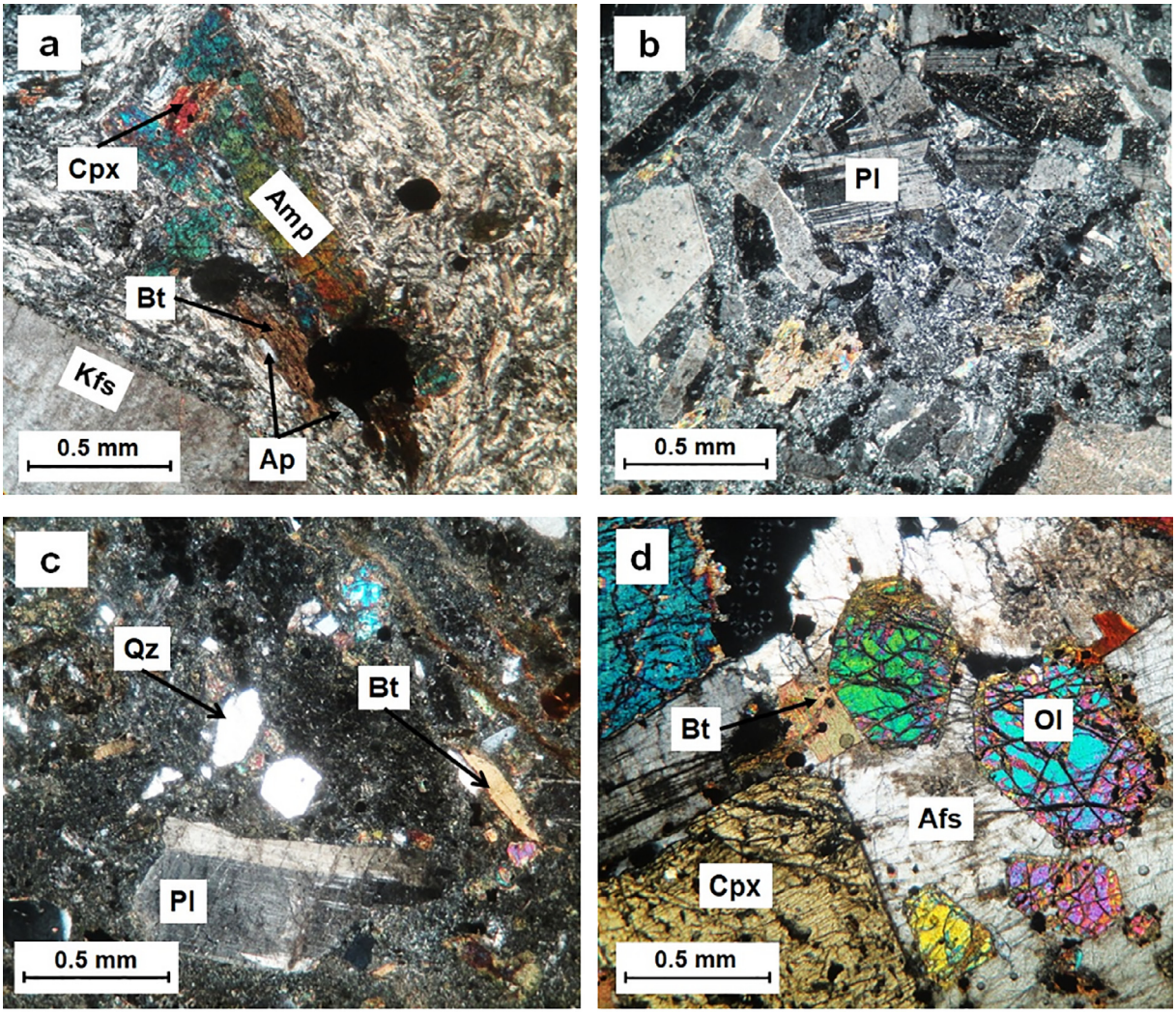

Fig. 5. Photomicrographs in crossed polarized light of extrusive rocks from the Lar porphyry Cu-Mo deposit. They are porphyritic in texture, phenocrysts are mainly plagioclase and K-feldspar with or without ferromagnesian minerals of amphibole, pyroxene, and biotite, and the groundmass is mainly feldspar that commonly is altered to phyllosilicates; (a) trachyte, (b) andesite, (c) pyroclastic, and (d) lamprophyre. Kfs: K-feldspar, Ap: apatite, Amp: amphibole, Bt: biotite, Cpx: clinopyroxene, Pl: plagioclase, Qz: quartz, Ol: olivine.

locally show poorly-developed microperthitic texture.

The lamprophyres dikes are minette, olivine minette, spessartite, kersantite and vogesite. They are fine- to coarse-grained and composed of green hornblende and brown biotite in variable proportions set in a groundmass of plagioclase in the spessartite and kersantite and K-feldspar in the vogesite. Moreover, the minette contains biotite and orthoclase. The micro-syenitic dikelets are fine-grained and composed of orthoclase, plagioclase, opaque minerals, and ferromagnesian minerals like clinopyroxene, amphibole, and biotite (Fig. 7a). Aplitic dikelets are fine-grained with micro-granular and aplitic texture and consist of orthoclase, plagioclase, and quartz as the main minerals, and apatite, titanite, and opaque minerals as accessory minerals (Fig. 7b).

6. Geochemistry of host rocks

Whole rock major and trace element concentrations of representative igneous rocks are presented in Table 1. The weight percent content of SiO_2, Al_2O_3, Fe_2O_3, MnO, MgO, CaO, Na_2O, K_2O, TiO_2, and P_2O_5 in all rocks ranges from 58.45 to 67.70, 17.35–18.50, 1.39–5.33, 0.01–0.08, 0.11–2.78, 0.48–3.42, 2.34–4.78, 5.37–9.43, 0.60–0.74, and 0.27–0.69, respectively. Geochemical studies indicate that the igneous rocks hosting the Lar porphyry Cu-Mo deposit are mainly syenitic, intermediate, and shoshonitic in composition (Figs. 8 and 9). These rocks are consistent with porphyry intrusions that formed from oxidized magmas (Fig. 10).

High K and Shoshonitic igneous rocks occur in a wide range of tectonic environments like continental arc, post-collisional arc, initial oceanic arc, late oceanic arc, and within-plat settings (Müller et al., 1992). Fig. 11 shows that igneous host rocks do fall in the field of arc-related tectonic setting. The ternary diagrams of Müller et al. (1992) discriminate the arc-related tectonic setting such as continent, post-collisional, initial oceanic and late oceanic arcs for potassic rocks. In Fig. 12a that discriminates the initial and late oceanic arcs from continent and post collisional arcs, the study samples fall in the field of continent arc and post-collisional environments.

In Fig. 12b that discriminates continent and post-collisional arcs, the samples fall in the field of post-collisional environments. The ternary diagram of Nb*50-Zr*3-Ce/P_2O_5 shows that the study samples belong to a post-collisional environment (Fig. 12b).

7. Alteration and mineralization

The visual footprint of hydrothermal alteration at the Lar Cu-Mo deposit contrasts with the surrounding unmineralized rocks due to hypogene and later supergene alteration (Fig. 13). The central part of the mineralized area is brown and outwards, the color is lighter.

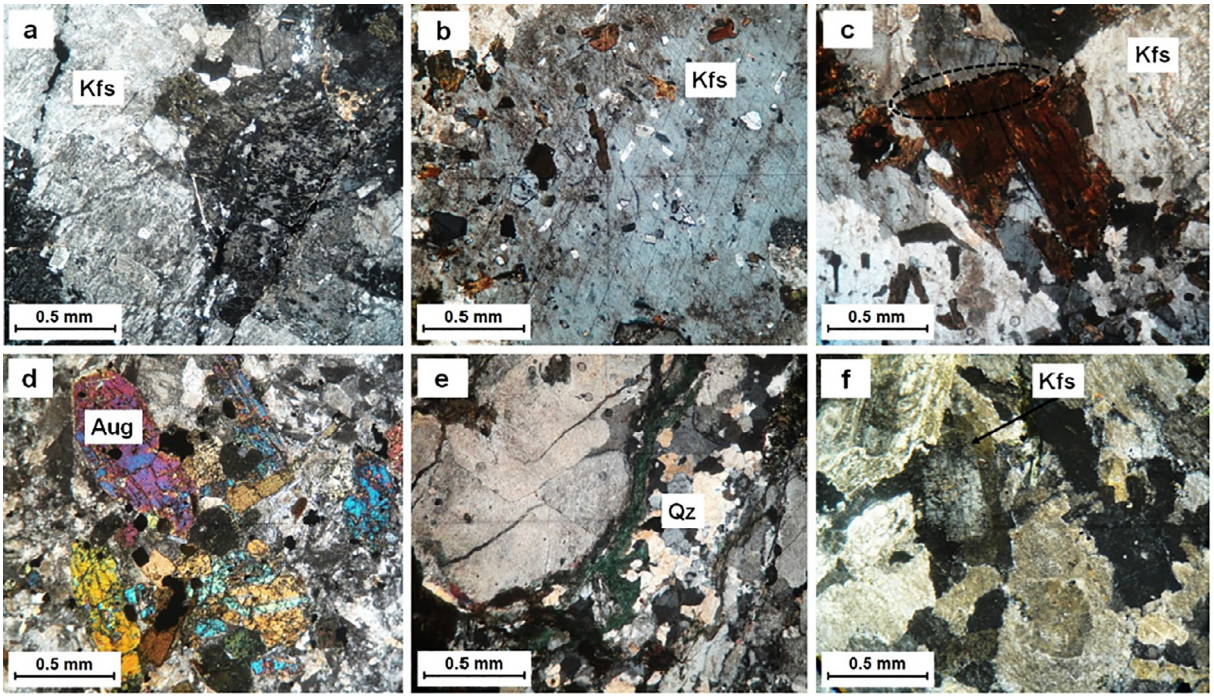

Fig. 6. Photomicrographs of the observed textures from the Lar intrusions in the mineralized area including: (a) perthitic K-feldspar megacryst, (b) K-feldspar poikilitically contain inclusions of plagioclase, biotite, titanite, apatite, pyroxene, and opaque minerals, (c) biotite with different size and shape is dark brown in color, (d) clinopyroxene phenocrysts with color interference, (e) a quartz veinlet, and (f) granular syenite. Kfs: K-feldspar, Qz: quartz, Aug: augite.

Volcanic rocks and hornfels are darker in color, especially on the eastern side of the mineralized area. The unmineralized shales and sandstones were locally affected by alteration on the western side, and also weather to a brownish color.

Supergene mineralization occurs in the upper two hundred meters in the study area, but it is not extensive. The supergene mineralization is characterized by the presence of iron hydroxides, Cu-carbonates, and secondary sulfide minerals, such as chalcocite and covellite, which partially replace hypogene chalcopyrite and bornite along fractures. Supergene mineralization is more intense in brecciated domains in faults and fractured zones, demonstrating that fractures played a significant role in controlling supergene mineralization. Supergene minerals are associated and mixed with hypogene sulfide minerals pyrite, chalcopyrite, and molybdenite from the surface to ~ 190 m depth.

Hypogene alteration is mainly characterized by silicification, including quartz vein and veinlets. As mentioned above, the Lar Cu-Mo mineralized area does not contain typical porphyry Cu-style alteration. However, there is evidence of potassic, propylitic, and phyllic hypogene alteration. The clearest manifestation of the potassic alteration and related mineralization is the development of quartz veins and veinlets that commonly contain hydrothermal orthoclase and biotite. Vein density rarely exceeds 20 vol% in the mineralized zone. Higher grade Cu zones are associated with quartz veins and veinlets. Generally, it is difficult to characterize the potassic alteration zone because the most abundant igneous mineral in the host rocks is orthoclase. The potassic alteration zone is also characterized by veins containing biotite and K-feldspar which may carry bornite, chalcopyrite, and/or molybdenite. Propylitic alteration is more widespread in the peripheral parts of the mineralized zone, especially in the hornfels and metavolcanic rocks where epidote, calcite, chlorite, and minor sericite partially replace magmatic pyroxene, hornblende, and biotite. Minor actinolite forms along the cleavage of the primary amphibole in a few samples. There are no classical alteration zones for phyllic and argillic alteration at Lar akin to those in most porphyry Cu systems (e.g., Gustafson and Hunt,

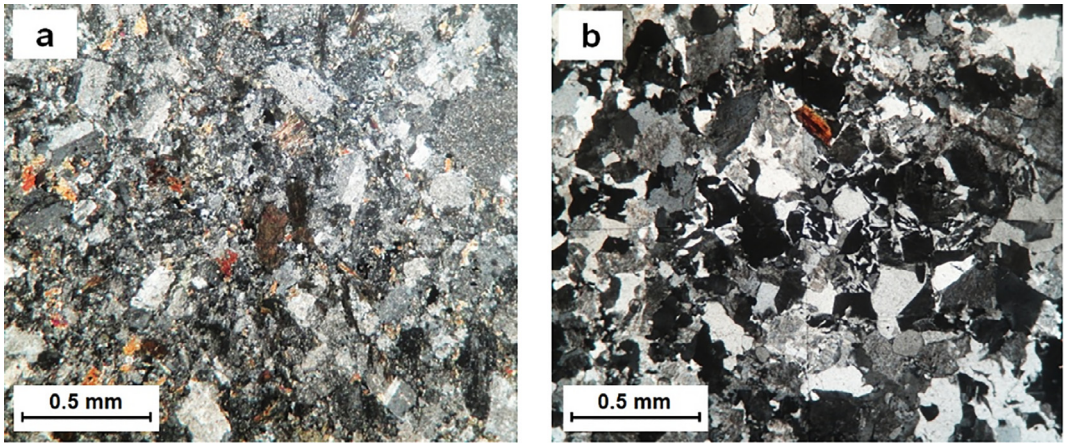

Fig. 7. Cross-polarized light photomicrographs of (a) micro-syenite with saussuritization of feldspars (turbid) evident and chloritic and phyllic alteration of ferromagnesian phases, and (b) aplite with granophyric intergrowths.

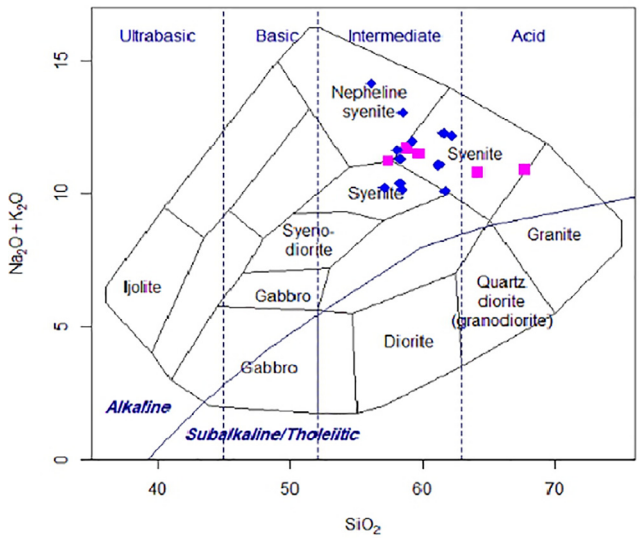

Fig. 8. Geochemical plots of the Lar porphyry Cu-Mo deposit igneous host rocks in plot of silica vs. total alkali classification diagram for intrusive rocks (Cox et al., 1979). Altered samples and least altered samples are shown in pink square and blue diamond, respectively. (For interpretation of the references to color in this figure legend, the reader is referred to the web version of this article.)

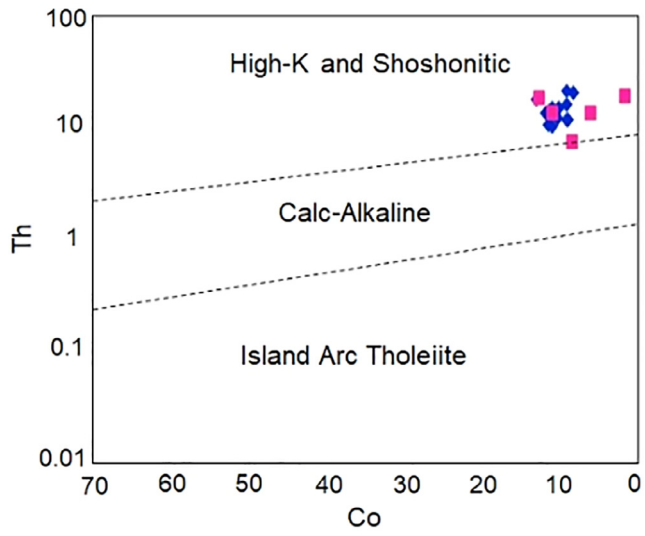

Fig. 9. Compositional characteristics of the Lar porphyry Cu-Mo deposit igneous host rocks in plot of Co (ppm) vs. Th (ppm) (after Hastie et al., 2007). Similar symbols as in Fig. 8.

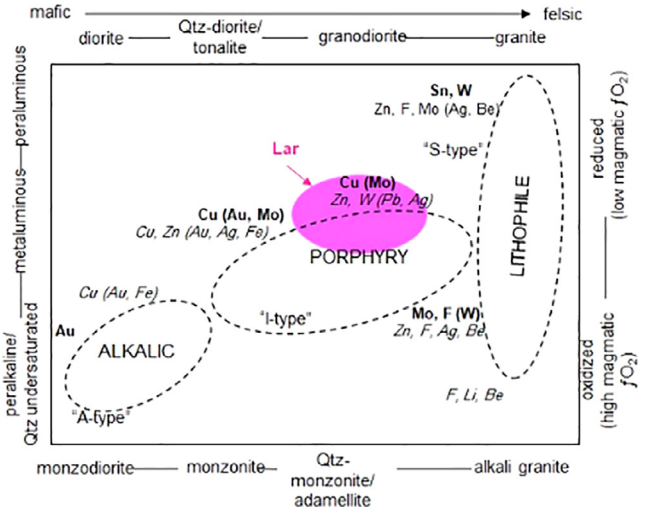

Fig. 10. Generalized scheme that links granitoid compositions and magmatic oxidation state to metal associations and intrusion-related ore deposit types (Robb, 2005) with location of the Lar porphyry Cu-Mo deposit igneous host rocks. Metal in bold reflect the important associations.

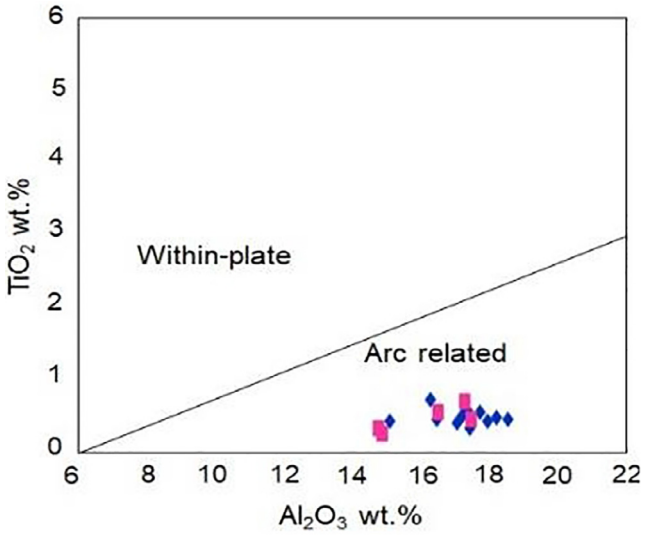

Fig. 11. Tectonic discrimination diagram of Al_2O_3 (wt%) vs. TiO_2 (wt%) for potassic igneous rocks (Müller et al., 1992) with location of the Lar porphyry Cu-Mo deposit igneous host rocks. Similar symbols as in Fig. 8.

1975). However, the majority of the feldspars are partially replaced by sericite and clay minerals, and mineralized and unmineralized quartz veins and veinlets are common in the study area. Argillic alteration occurs locally in outcrops and at shallow depths in the Lar system. This alteration, characterized by clay minerals, iron hydroxides, and Cu carbonates, likely formed through weathering processes.

Diagram of (2Ca + Na + K)/Al versus K/Al molar ratios (Fig. 14) is commonly used to evaluate K-metasomatism and mass transfer in related to hydrothermal alteration minerals from whole-rock geochemical data (Stanley and Madeisky, 1994; Madeisky, 1996; Warren et al., 2007; Mauk and Simpson, 2007; Booden et al., 2011). In this diagram, fresh felsic igneous rocks will usually plot on or near to plagioclase-K-feldspar line and fresh intermediate to mafic rocks plot progressively to the right of this line in proportion to the amounts of Ca-bearing minerals they contain. This diagram shows that the most altered rocks from the study area plot in an array between plagioclase/albite and K-feldspar/biotite, whereas unaltered rocks plot to the right of that array (Fig. 14). This suggests that the altered rocks show limited potassium gain.

Hypogene mineralization can be divided into: (1) quartz-sulfide veins and veinlets, (2) sulfide veinlets, and (3) disseminated sulfides. These mineralization types occur throughout outcrops of the intrusion in the northeastern, eastern, southeastern, and in the deeper parts of the Lar porphyry Cu-Mo deposit, where stockwork mineralization intensifies.

Unmineralized quartz veins and veinlets have a dominant NW-SE direction (Fig. 15), and vary from 0.5 cm to 2 m in width. These veins consist predominantly of massive to granular milky and crystalline quartz grains (Fig. 16a). In general, barren veins are more variable in width, and extend for longer distances than mineralized veins. K-feldspar is the main alteration mineral around these veins. Barren quartz veins are present in many rock types throughout the Lar porphyry Cu-Mo deposit.

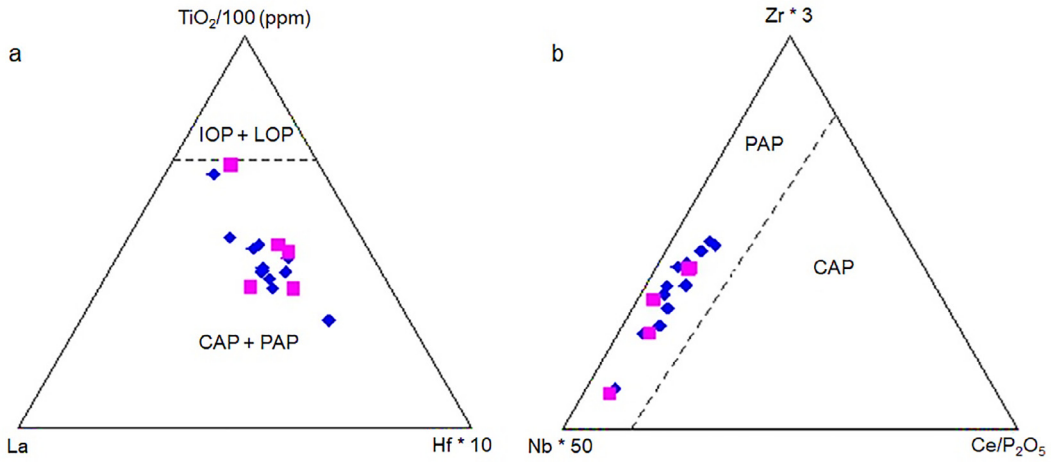

Fig. 12. Tectonic discrimination diagram of (a) La-TiO_2/ 100-Hf*10 and (b) Nb*50-Zr*3-Ce/P_2O_5 for potassic igneous rocks (Müller et al., 1992) with location of the Lar porphyry Cu-Mo deposit igneous host rocks (IOP: Initial oceanic arc, LOP: Late oceanic arc, CAP: Continental arc, PAP: Post-collisional arc). Similar symbols as in Fig. 8.

The density of mineralized quartz veins is low in the northern and southern parts of the Lar area; most of the mineralized quartz veins and veinlets are concentrated in the central part of the Lar porphyry Cu-Mo deposit as true stockworks. The mineralized veins and veinlets have various orientations, but they mostly strike NNW-SSE (Fig. 15). Their thickness varies from < 1 cm to 10 cm (Fig. 16a).

The quartz-sulfide veins and veinlets consist of milky and crystalline quartz with various kinds of mineralization as follows: (1) quartz-chalcopyrite (Fig. 16b) and quartz-chalcopyrite-bornite (2) quartz-chalcopyrite-molybdenite (Fig. 16c), (3) quartz-molybdenite, (4) quartz-chalcopyrite-molybdenite-pyrite, and (5) quartz-chalcopyrite-bornite-molybdenite. Quartz-chalcopyrite veins and veinlets are variable in size and contain subhedral to anhedral chalcopyrite in varying quantity. They are the most abundant mineralized veins in the Lar porphyry Cu-Mo deposit. The quartz-chalcopyrite-molybdenite veins and veinlets consist mainly of quartz, anhedral to subhedral chalcopyrite and molybdenite. At some localities, sulfide-bearing veins cut earlier barren quartz veins. Quartz-molybdenite veins are thinner than other mineralized veins, and they are most abundant in the shallow part of the Lar porphyry Cu-Mo deposit. Quartz in the quartz-molybdenite veins is anhedral, more coarse-grained quartz in other veins, gray in color, and contains molybdenite stringers. In the quartz-chalcopyrite-molybdenite-pyrite veins and veinlets, brecciated euhedral pyrite grains are surrounded by chalcopyrite and molybdenite. The quartz-chalcopyrite-bornite and quartz-chalcopyrite-bornite-molybdenite veinlets all vary in size. In such veins, anhedral chalcopyrite and bornite grains are typically interlocked. The chalcopyrite is replaced by supergene chalcocite and covellite at greater depth and malachite, azurite, and iron hydroxides at shallow depth and occur as quartz-chalcopyrite-molybdenite-bornite ± covellite ± chalcocite veins and quartz-malachite, quartz-azurite (Fig. 16d), quartz-malachite-azurite (Fig. 16e), and quartz-iron hydroxides (Fig. 16f) veins. Sericite is common around the veins and veinlets.

Based on petrographic examination and cross-cutting relationships, at least five main groups of sulfide veins and veinlets are recognized. They are: (a) chalcopyrite veinlets that are 1.7 cm to < 1 mm thick (Fig. 17a and d), (b) bornite-chalcopyrite veinlets that are 1 mm thick (Fig. 17b and e) with common supergene chalcocite ± covellite, (c) molybdenite veinlets that are < 1 mm thick (Fig. 17c), (d) hematite-bornite veinlets that are < 1 mm thick (Fig. 17f) and (e) chalcopyrite

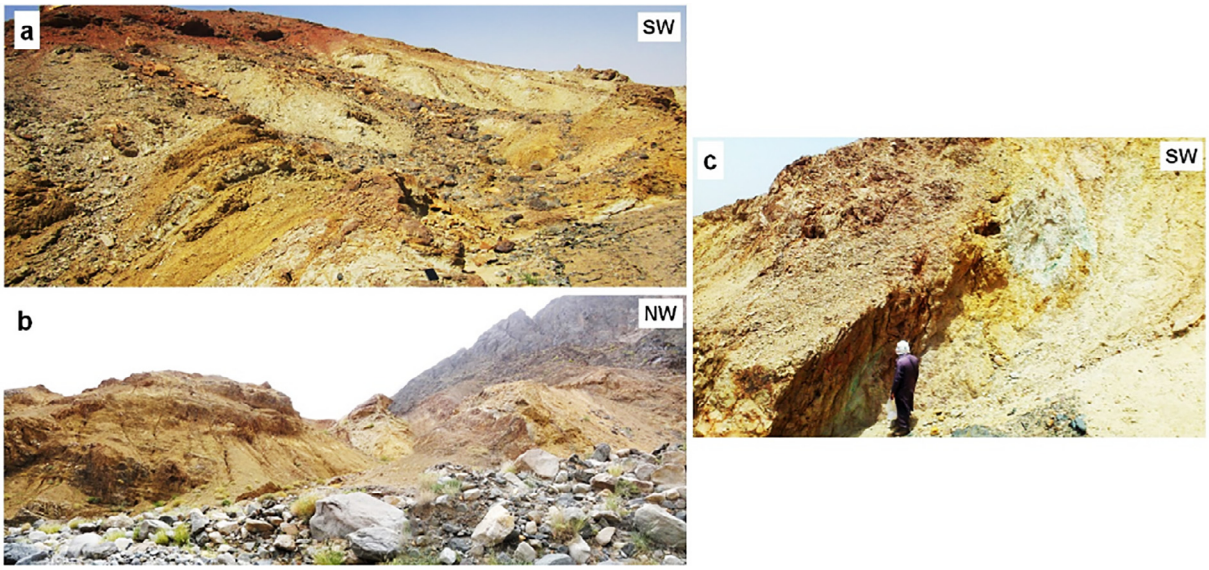

Fig. 13. Field photographs of the mineralized areas (based on Fig. 2-a), (a) the main mineralized area 1, (b) mineralized area 2, and (c) mineralized area 3. These areas has brown to cream color due to supergene and hypogene alteration types.

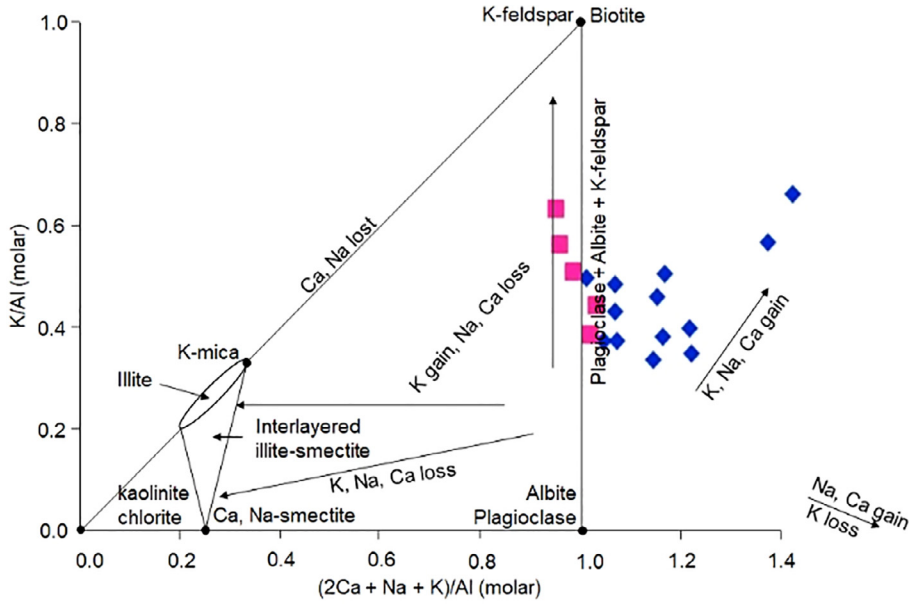

Fig. 14. Molar element ratio plot of (2Ca + Na + K)/Al vs. K/Al (after Madeisky, 1996) with location of the Lar porphyry Cu-Mo deposit igneous host rocks. Mass transfer processes are shown with arrows that vector toward associated alteration minerals (Warren et al., 2007). Similar symbols as in Fig. 8.

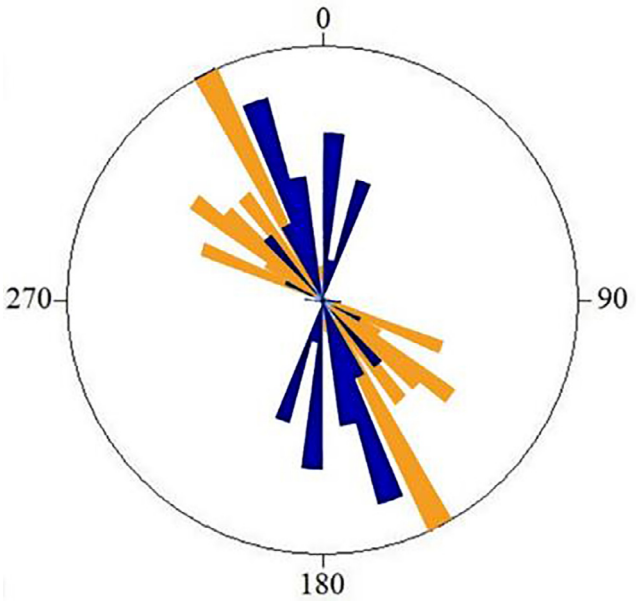

Fig. 15. Rose diagram for barren quartz veins and mineralized quartz veins in orange and blue, respectively. (For interpretation of the references to color in this figure legend, the reader is referred to the web version of this article.)

veinlets that are < 1 mm thick ± supergene covellite (Fig. 17g).

Disseminated mineralization occurs in syenitic to monzonitic intrusions, especially in association with the quartz veins carrying chalcopyrite, bornite, molybdenite, magnetite and rare pyrite, hematite and enargite as hypogene minerals and covellite, chalcocite, malachite, azurite and rare digenite and native copper as supergene minerals (Fig. 18). Pyrite is brecciated and presented in minor amounts as small subhedral disseminated grains (about 0.2 mm) in the host rock and among the other minerals (Fig. 18a).

Chalcopyrite and bornite are the most abundant sulfide minerals and they are found as veins, veinlets, and dispersed small to coarse grains (0.1–greater than3 mm). Along crystal boundaries in these sulfides, covellite and digenite are common. Chalcopyrite may be intergrown with bornite (Fig. 18b), and generally occurs at shallower depths than bornite. Bornite is the dominant sulfide deeper in the porphyry system. Molybdenite occurs in quartz veinlets as anhedral grains (0.2–greater than3 mm) (Fig. 18c).

Based on the paragenetic sequence in Fig. 19, the primary sulfides are pyrite, chalcopyrite, molybdenite, and bornite followed by magnetite, and enargite. Chalcocite, covellite, minor native copper, malachite, azurite, and iron hydroxides are secondary minerals; and are developed from the primary ones through weathering. Quartz is the dominant hydrothermal gangue mineral.

8. Stable isotope data

8.1. Sulfur

The isotopic composition of sulfur was obtained for four pairs of chalcopyrite-bornite and chalcopyrite-molybdenite in the quartz-sulfide veins and sulfide veinlets and disseminations (Table 2). The $\delta^{34}S$ values for the measured sulfide minerals from quartz-sulfide veins and disseminated sulfide in ore-bearing porphyry (porphyritic syenite) range from 0.3 to -1.8‰ and -0.4 to -0.6‰, respectively (Table 2).

8.2. Oxygen

Oxygen isotope data were obtained from pure quartz from the veins and whole rocks from less-altered syenite and altered syenites (Table 3). K-feldspar (50–65%) and plagioclase are primary minerals in all study syenites. Quartz presents in all samples. Samples of RM16, RM15 and RM1 are weakly altered to potassic and argillic. Other samples including RM707 (phyllic) and RM120 and RM501 (propylitic) are soft rocks due to intense alteration. The $\delta^{18}O$ values of two pure quartz samples from the mineralized veins are 11.5 and 9.5‰ and the $\delta^{18}O$ value of one pure sample from an unmineralized quartz vein is 9.9‰. The $\delta^{18}O$ values of less-altered and altered syenites range from 8.4 to 13.0‰.

9. Re-Os geochronology on molybdenite

Re-Os dating of molybdenite provides robust primary radiometric ages (McCandless and Ruiz, 1993; McCandless et al., 1993; Stein et al., 2001; Stein et al., 2003; Barra-Pantoja, 2005; Stein, 2014). The

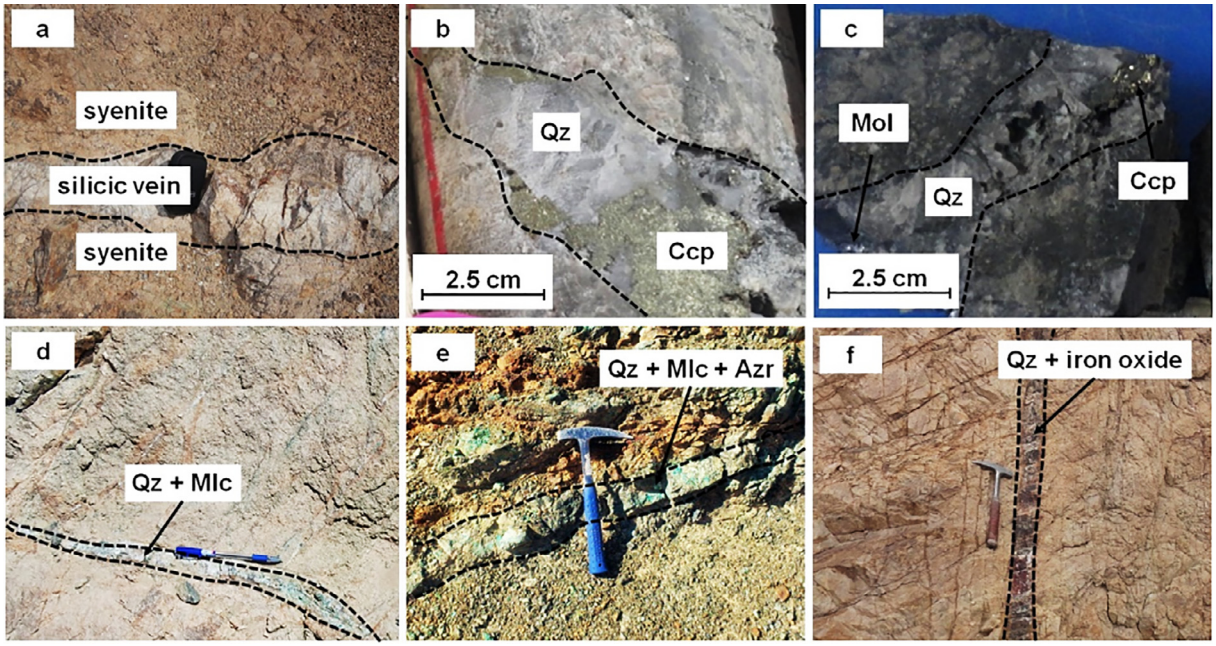

Fig. 16. Photographs of (a) barren quartz vein, (b) quartz - chalcopyrite vein, (c) quartz - chalcopyrite - molybdenite vein (d) quartz - malachite vein, (e) quartz - malachite - azurite vein, and (f) quartz - iron hydroxides vein. Ccp: chalcopyrite, Mol: molybdenite, Mlc: malachite, Qz: quartz, Azr: azurite.

concentrations of Re and Os and Re-Os dating of molybdenite from the Lar porphyry Cu-Mo deposit are shown in Table 4. The total Re, Os, and ^{187}Os concentrations of molybdenite range from 5.558 to 289.8 ppm, 0.148 to 0.224 ppb, and 1.730 to 96.98 ppb, respectively. The determined ages of two molybdenites in argillically and phyllically altered host rocks are 29.72 ± 0.11 Ma and 31.95 ± 0.11 Ma. These ages are significantly different, and apparently capture two distinct mineralization episodes. Further, the two ages suggest that the Lar system was active for at least 2.0 Ma. According to K/Ar dating on biotite (one sample) and whole rocks (two samples), the age of the intrusive rocks ranges from 27.8 ± 3 to 32. 8 ± 3 Ma (Camp and Griffis, 1982). The Re-Os ages for molybdenite overlap the K/Ar dates, are coeval with the Lar magmatism, and provide more precise ages that can be linked directly to the mineralization. These similar ages of the mineralization and the igneous rocks indicate that the mineralization is associated with the syenitic and monzonitic intrusions.

10. Discussion

10.1. Source of magma

K-rich magmas of shoshonitic affinities are typically emplaced in post-collisional environments and active continental margins (Castro et al., 2013). The model favored for generating these magmas is partial melting of modified peridotites involving breakdown of hydrous minerals such as phlogopite and pargasite which were formed by reaction between mantle and water rich silicic melts (Castro et al., 2013). Generally, K-rich magmatism in a post-collisional tectonic setting is associated with strike-slip faults and is generated from enriched mantle sources and/or metasomatized lithospheric mantle, and it produces shoshonitic lavas, lamprophyres, and K-rich granitites (Bonin et al., 1998; Vaughan and Sacrow, 2003; Seifert, 2008). Strike-slip faults are capable of channeling mantle fluids and also generating deep lithospheric heat. They can create a space for deep-seated magmas that make their way upward along the faults, as a result of decompression melting (Pirajno, 2010).

10.2. Mineralization type

The Lar mineralization is believed to be porphyry Cu-Mo style mineralization (Figs. 20–22) based on its metal content (0.16% Cu and 0.01% Mo on average), size (about 1.5 by 0.5 km in plain view), sulfide assemblage, and its association with intermediate intrusions. However, there are significant differences between the Lar porphyry Cu-Mo deposit and the typical porphyry systems as follows:

At Lar, the mineralization is mainly contained in NW-striking quartz veins and veinlets. In contrast, in many porphyry systems, vein and veinlets show a radial or concentric pattern, implying that, the local stress regime around the intrusive complex can control vein orientation, though in a few cases, regional stress predominates, resulting in a strong preferred orientation to the veins or sheeted veins (Cooke et al., 2014).

Lar lacks some alteration and zoning that commonly occurs in other porphyry Cu-Mo deposits. The Lar porphyry host rocks are not pervasively altered and rarely contain primary quartz and secondary K-feldspar and biotite. The Lar porphyry deposit is mainly characterized by silicic alteration rather than potassic alteration. Pyrite is typically the dominant sulfide in many porphyry systems which reflects the huge abundance of sulfur in those systems. By contrast the overall sulfur and pyrite contents are low at Lar.

In contrast to Cu porphyries with an aplitic quartz-feldspar groundmass, the Lar syenitic intrusions are mainly porphyritic in texture with a feldspar dominant coarse-grained groundmass and about 30% megacrysts.

The Lar porphyry Cu-Mo deposit also differs in its tectonic setting in comparison with many other porphyries worldwide. The Lar intrusive rocks are shoshonitic and related to collision and post-collision events of the Lut and Afghan blocks. Formation of hydrothermal mineral deposits is often the result of interaction among several key processes including structural, hydrological, lithological, and geochemical processes (e.g., Hobbs et al., 2000; Ord et al., 2002; Zhang et al., 2008). Among them, structural processes represent one type of critical control on mineralization. Furthermore, it is generally accepted that porphyry Cu deposits are structurally controlled, but opinions vary as to the relative importance of regional versus local fault systems (Cooke et al., 2005; Berger et al., 2008). At Lar, evidence such as the intrusion shape

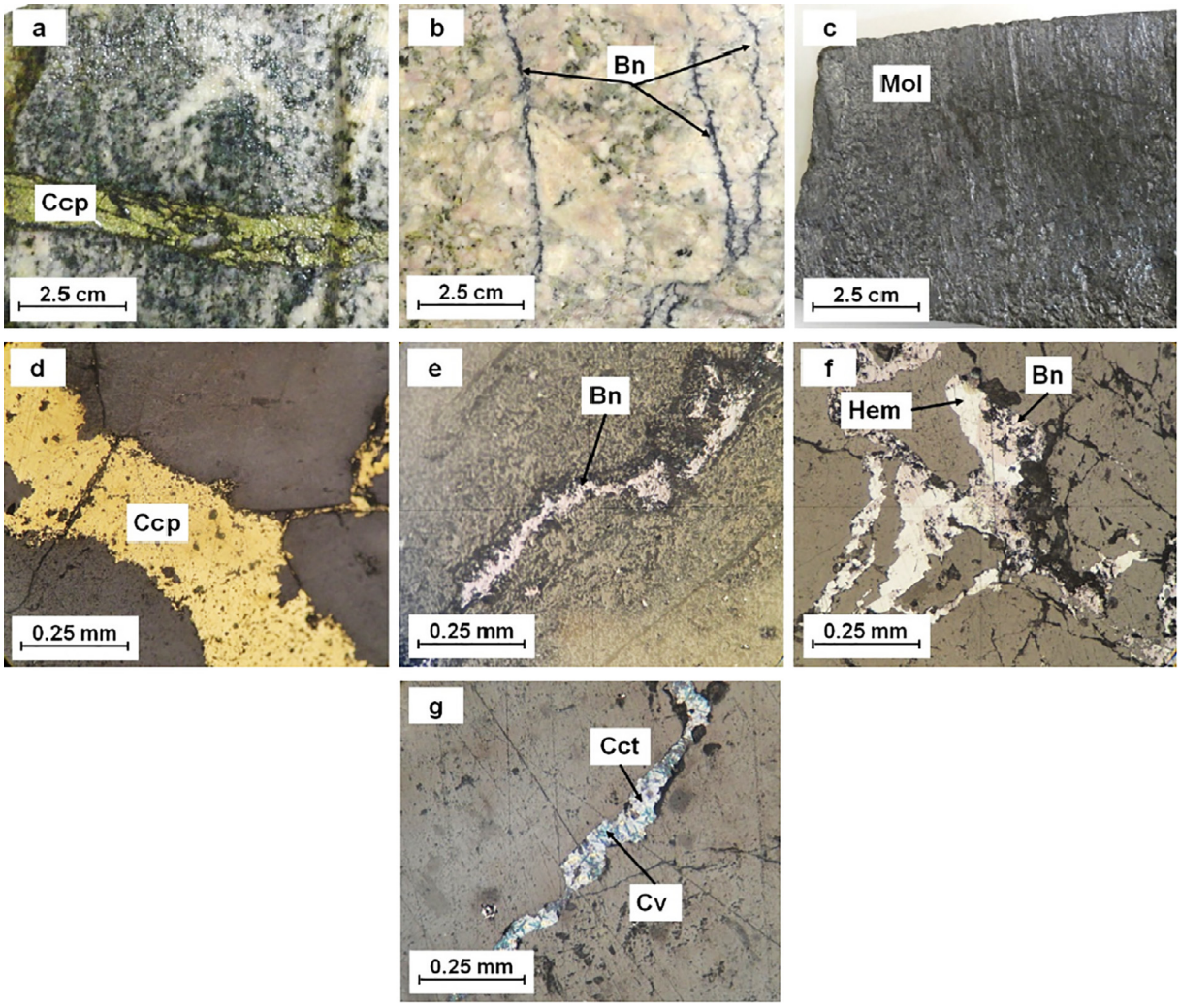

Fig. 17. Hand samples of (a) chalcopyrite vein, (b) bornite vein, (c) molybdenite vein. Photomicrographs in reflected plane light of (d) chalcopyrite veinlet, (e) bornite veinlet, (f) hematite and bornite veinlet, and (g) covellite and chalcopyrite veinlet. Bn: bornite, Ccp: chalcopyrite, Hem: hematite, Cv: covellite, Mol: molybdenite.

and distribution of this type of magmatism in the SSZ with respect to the faults suggests the involvement of an active strike slip fault system for emplacement of the igneous rocks and formation of the related mineralization. The concentration of alteration in a NNW-SSE orientation and the mineralized quartz vein arrays that strike NNW-SSE also suggests involvement of the strike-slip fault system.

10.3. Sulfur isotopes

The sulfur isotope data of the Lar porphyry Cu-Mo deposit show a very narrow range of $\delta^{34}S$ values, suggesting a homogeneous fluid and that the sulfur is most likely related to mantle-dominated igneous sources (Fig. 23). These values show little variability, and are typically near 0‰, consistent with values of igneous sulfur (0 ± 3‰, Chaussidon et al., 1987) and most porphyry systems (0 ± 5‰, Ohmoto and Rye, 1979).

Samples RM22 and RM108 are not useful for geothermometry because primary sulfides such as molybdenite, chalcopyrite, and bornite are associated with secondary sulfides of covellite and chalcocite, indicating that the primary sulfide minerals were altered by supergene processes. Samples RM3 and RM4 only contain primary sulfides; the sulfide pairs are considered to be in equilibrium at the time of their formation and should yield reasonable temperatures using isotope fractionation thermometry. Using published molybdenite-chalcopyrite (Suvorova, 1974) and chalcopyrite-bornite (Ohmoto and Rye, 1979) fractionation factors, the calculated temperature for the molybdenite-bornite pair in the quartz-sulfide vein is 779 °C, and for disseminated sulfides of the chalcopyrite-bornite pair, it is 753 °C.

10.4. Oxygen isotopes

The isotopic fractionation factor of Clayton et al. (1972) and temperature of 779°C were applied to calculate $\delta^{18}O_{H2O}$ value in equilibrium with quartz in mineralized quartz veins. The assumed temperature of 779°C is based on the $\Delta^{34}S$ value for the molybdenite-chalcopyrite pair using the fractionation factor of Suvorova (1974). According to these calculations, the $\delta^{18}O_{H2O}$ values in equilibrium with quartz in mineralized quartz veins are 11.2 and 9.3‰, and the calculated value of $\delta^{18}O_{H2O}$ in equilibrium with quartz in a barren quartz vein is 9.6‰.Two samples from the quartz veins have calculated $\delta^{18}O_{H2O}$ values in the range magmatic waters and one sample has a slightly greater $\delta^{18}O_{H2O}$ value than the magmatic waters. The assumed temperature that is based on the molybdenite-chalcopyrite pair thermometry is notably high relative to reported temperatures for the magmatic waters. With lower temperatures (for example 500 °C), the calculated $\delta^{18}O_{H2O}$ values range from 7.3 to 9.2‰, which remains in the range of magmatic water values (Table 2). Only at temperatures of about 100 °C, do the calculated waters in equilibrium with quartz have

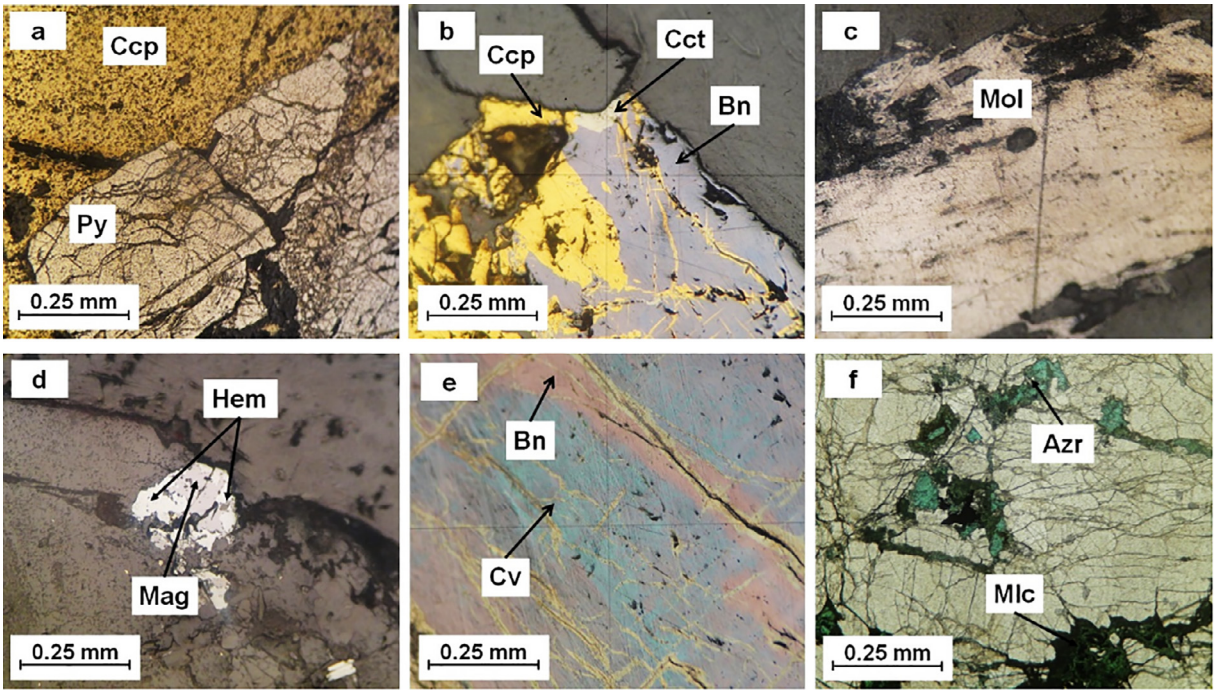

Fig. 18. Photomicrographs of some ore minerals in the Lar porphyry Cu-Mo deposit. Bn: bornite, Cct: chalcocite, Cv: covellite, Ccp: chalcopyrite, Py: pyrite, Mol: molybdenite, Hem: hematite, Mag: magnetite, Mlc: malachite, Azr: azurite.

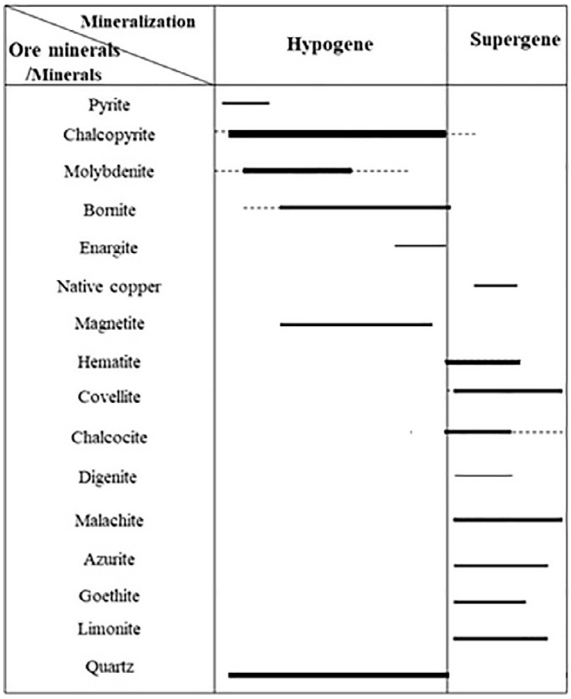

Fig. 19. Schematic representation of paragenetic sequence in the Lar porphyry Cu-Mo deposit.

$\delta^{18}O_{H2O}$ values that are similar to those of meteoric waters (Table 2).

The general range of whole rock $\delta^{18}O$ values in syenites and trachytes is about 6 to 8‰ (Taylor and Sheppard, 1986). Whole rock samples in this study have relatively enriched $\delta^{18}O$ values with an average value of 10.6‰, showing significant enrichment in ^{18}O compared to the typical values for syenites and trachytes. For igneous rock series where oxygen isotope variations are larger than 1‰, processes in addition to crystal fractionation must be strongly suspected as being involved. In most cases, it is only in the near-surface sedimentary and weathering environments, and in hydrothermal systems that oxygen isotope fractionations are big enough to produce sufficiently large $\delta^{18}O$ changes in the rocks (Taylor and Sheppard, 1986). According to Turi and Taylor (1971), a granodioritic stock with a $\delta^{18}O$ value of 7.4‰ was emplaced into more ^{18}O-rich metamorphic rocks ($\delta^{18}O$ = 20.0‰), which caused considerable enrichment in ^{18}O for at least 150–200 m inward from the margins of the granodiorite pluton. They concluded that this effect could in part be due to sub-solidus metamorphic-hydrothermal and water/rock interaction produced by inward migration of high-^{18}O fluids.

Altered igneous rocks are depleted in ^{18}O under most geological condition through exchange with meteoric waters at intermediate to high temperatures (Taylor, 1971(, whereas the igneous rocks can be only enriched by low temperature meteoric waters. The enriched $\delta^{18}O$ values of this study's whole rocks cannot be explained by interaction with intermediate to high temperature meteoric hydrothermal waters. The enriched $\delta^{18}O$ values also cannot be explained by interaction with magmatic waters, because the maximum $\delta^{18}O$ value of magmatic waters is approximately 10‰. If a syenite with a $\delta^{18}O$ value of about 8.0‰ interacted with magmatic waters with a $\delta^{18}O$ value of 10‰, the syenite could be slightly enriched in ^{18}O, probably by approximately 0.5‰. Only magmatic waters that are enriched in ^{18}O via exchange with metasedimentary rocks (water/rock interaction) could produce the hydrothermal fluids with greater $\delta^{18}O$ values (Field and Fifarek, 1985). This new hydrothermal water could sharply increase the ^{18}O in the igneous rocks in margin.

The final isotopic composition of altered rocks after equilibration with hydrothermal waters is a function of the isotopic composition of the water and initial rock, the water/rock ratio and the temperature of equilibration. The final isotopic compositions of the study rocks were calculated by equation of Taylor (1977) at different temperatures and water/rock ratios for meteoric and magmatic waters, and for waters that are in equilibrium with the mineralized and unmineralized quartz. The equations are $W/R_{closed} = (\delta fR - \delta iR)/[\delta iW - (\delta iR - \Delta_{R-W})]$ and $W/R_{open} = Ln\ (W/R_{closed} + 1)$ where f = final, i = initial, W = water, R = rock and $\Delta_{R\text{-}W} = \delta fR - \delta fW$. The Alkali feldspar-water fractionation factor of O'Neill and Taylor (1969) is used in the above

Table 2
Sulfur isotope compositions of mineral pairs and estimated temperature of hypogene assemblage in the Lar porphyry Cu-Mo deposit.

Sample Number	Host	Paragenesis	Minerals	Sulfur content (%)	$\delta\ ^{34}S_{V\text{-}CDT}$ (‰)	T (°C)
RM222	quartz vein	Quartz + chalcopyrite + molybdenite + bornite ± covellite ± chalcocite	Chalcopyrite	35.13	0.3	–
			Molybdenite	37.96	-1.8	
RM108	quartz vein	Quartz + chalcopyrite + bornite ± chalcocite	Chalcopyrite	25.48	-0.5	–
			Bornite	27.73	-1.6	
RM3	quartz vein	Quartz + chalcopyrite + molybdenite	Chalcopyrite	15.66	-0.5	779
			Molybdenite	3.20	-0.5	
RM4	syenite	Chalcopyrite + bornite	Chalcopyrite	10.85	-0.4	753
			Bornite	10.02	-0.6	

Table 3
Oxygen isotope compositions of the Lar porphyry Cu-Mo deposit.

Sample	Rock type	Mineral	Alteration	Measured isotopic values	$\delta^{18}O$ (‰) Calculated water		
				$\delta^{18}O_{VSMOW}$ (‰)	779 °C	500 °C	100 °C
RM16	Syenite	Whole rock	Fresh	8.4	–	–	–
RM15	Syenite	Whole rock	Potassic	9.5	–	–	–
RM707	Syenite	Whole rock	Phyllic	13.0	–	–	–
RM120	Syenite	Whole rock	Propylitic	11.4	–	–	–
RM1	Syenite	Whole rock	Weak argillic	8.8	–	–	–
RM501	Syenite	Whole rock	Propylitic	12.4	–	–	–
RM222	Mineralized quartz vein	Quartz	Phyllic	11.5	[I]*11.2	[II]9.2	-9.4
RM108	Mineralized quartz vein	Quartz	Potassic	9.6	[I]*9.2	[II]7.3	-11.3
RM12	Barren quartz vein	Quartz	Potassic	9.9	[I]**9.6	[II]7.6	-11.0

*Based on sulfide pairs thermometry as lowest temperature of the quartz veins.
**Based on sulfide pairs thermometry of mineralized quartz veins in potassic alteration zone.
[I] 1000 lnα Quartz – water = 2.51 ($10^6/T^2$) – 1.96 (T = 500 – 750 °C), Clayton et al. (1972).
[II] 1000 lnα Quartz – water = 3.38 ($10^6/T^2$) – 3.40 (T = 200 – 500 °C), Clayton et al. (1972).

Table 4
Re-Os isotope data for molybdenite at the Lar porphyry Cu-Mo deposit.

Minerals	Host rock	Alteration	Re (ppm)	^{187}Os (ppb)	Common Os (ppb)	Age (Ma)
Molybdenite	Syenite	Argillic	5.558	1.730	0.224	29.72 ± 0.11
Molybdenite	Syenite	Phyllic	289.8	96.98	0.148	31.95 ± 0.11

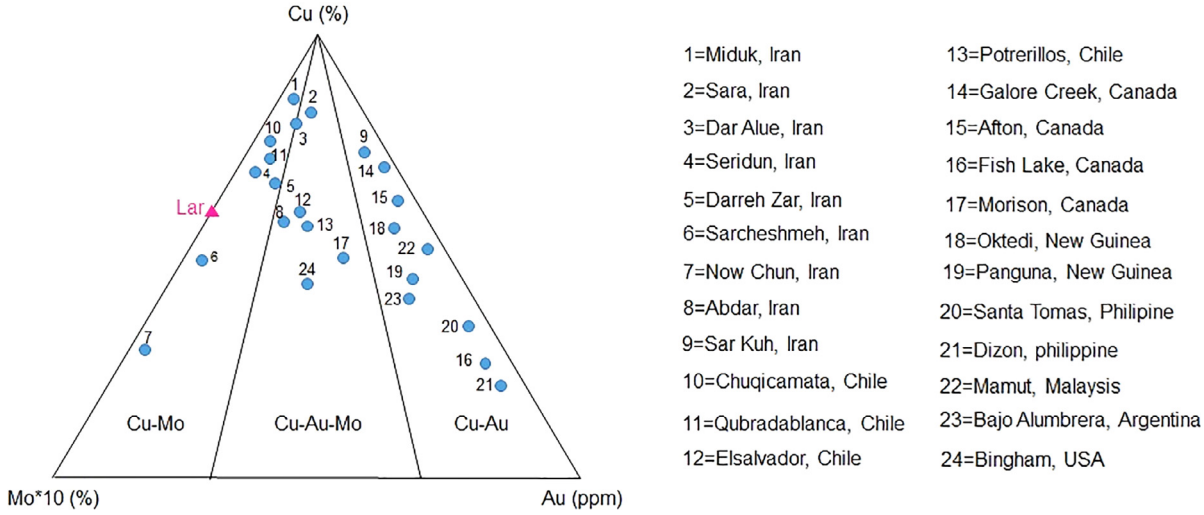

Fig. 20. Separation diagram of porphyry Cu deposits (Cox and Singer, 1988). The Lar porphyry Cu-Mo deposit is located in the field of porphyry Cu-Mo deposits. Data for Iranian and other world porphyry deposits are from Shafiei and Shahabpour (2008), Soltaninejad and Shafiei (2014), and Vila and Sillitoe (1991), respectively.

equations.

Calculated curves showing isotope and open system water/rocks trajectories are shown in Fig. 24. These trajectories are constructed assuming different temperatures, fluids, and molar oxygen water/rock ratios (up to 10). The $\delta^{18}O$ value of initial rocks is assumed to be 8‰, which is similar to values of the fresh and less-altered rock of the study area. The $\delta^{18}O_{H2O}$ values are assumed to be –8, 8, and 10‰ for Fig. 24a, b, and c, respectively.

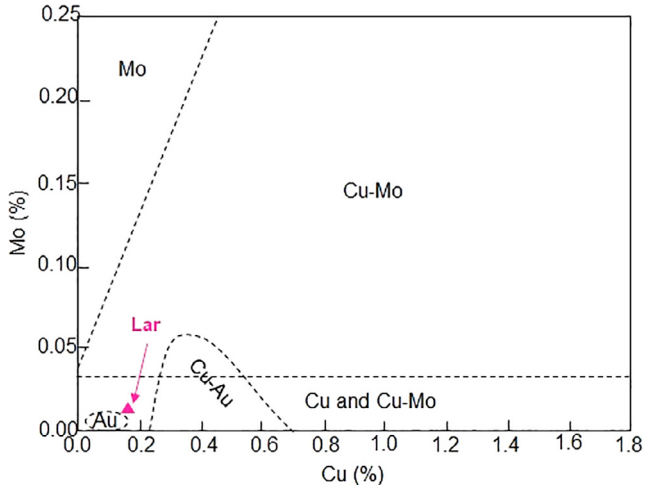

Fig. 21. Mo vs. Cu grades in porphyry deposits (modified from Kirkham and Sinclair, 1995; Sinclair, 2007). The Lar porphyry Cu-Mo deposit is located in the field of porphyry Cu-Mo deposits.

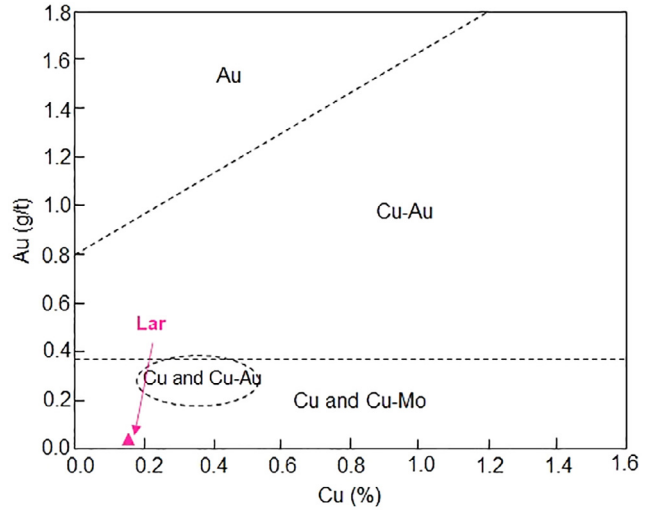

Fig. 22. Au vs. Cu grades in porphyry deposits (modified from Kirkham and Sinclair, 1995; Sinclair, 2007). The Lar porphyry Cu-Mo deposit is located in the field of porphyry Cu-Mo deposits.

By assuming of value for meteoric water ($\delta^{18}O = -8‰$), the $\delta^{18}O$ values of the altered rocks in the study area could be explained by temperatures of < 100 °C (Fig. 24a). By assuming magmatic water or enriched magmatic water ($\delta^{18}O_{H2O} = 8‰$ and $\delta^{18}O_{H2O} = 10‰$, respectively), the $\delta^{18}O$ values of the altered rocks in the study area could be explained by temperatures of 300–500 °C, and 400–700 °C, and Water/rock ratios of more than 1 (Fig. 24b and c).

With the calculated temperatures by the sulfide pairs, the calculated waters in equilibrium with the quartz veins and the $\delta^{34}S$ values of the measured sulfide minerals are more similar to those of magmatic waters, therefore, reaction with meteoric water ($\delta^{18}O_{H2O} \sim -8‰$) cannot easily account for the oxygen isotope composition of the ore-forming fluids in equilibrium with the Lar altered syenite (Fig. 24); but an interaction of magmatic fluids ($\delta^{18}O_{H2O} \sim 8‰$ or 10‰) with host rocks is sufficient to explain the fluid oxygen isotope signatures (Fig. 24b and c).

11. Conclusions

- The Lar deposit is a structurally controlled, sub-economic porphyry Cu-Mo deposit with 0.16% Cu and 0.01% Mo on average.

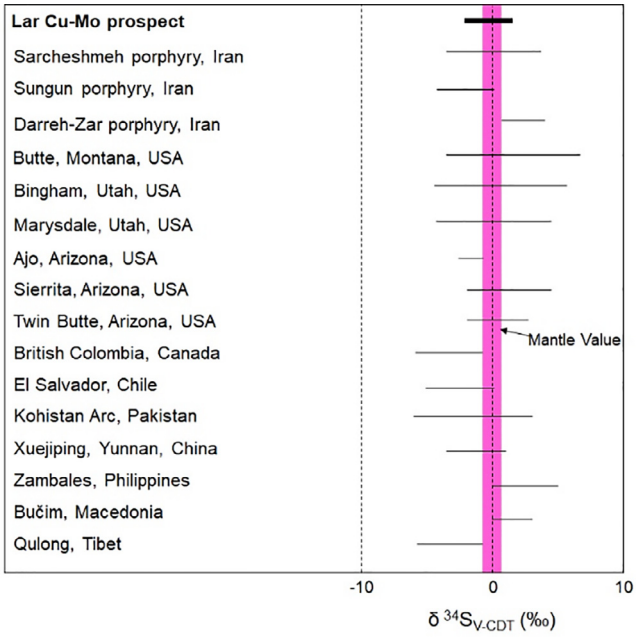

Fig. 23. Comparison of the $\delta^{34}S$ compositions in the Lar porphyry Cu-Mo deposit with the other well-known porphyry Cu deposits. Data for other deposits: Sarcheshmeh (Maanijou et al., 2013), Sungun (Calagari, 2003), Darreh-Zar (Parsapoor et al., 2014), Butte, Bingham, Marysdale, Ajo, Sierrita, Twin Butte, El Salvador (Ohmoto and Rye, 1979), British Columbia (Deyell, 2005), Kohistan Arc (Kausar, 1992), Xuejiping (Chengbiao et al., 2008), Zambales (Imai, 2005), Bučim (Serafimovski et al., 2016), and Qulong (Meng et al., 2006).

- The Lar porphyry Cu-Mo deposit in the LIC is genetically related to post-collisional magmatic activities in the Sistan suture zone. The igneous rocks in the LIC include intrusions, flows, and tuffs. They are mainly basic to intermediate in composition and shoshonitic. The main rocks in the Lar porphyry Cu-Mo deposit are porphyritic syenite and monzonite that occur as stocks. Aplite and micro-syenite dikes are barren and post-date the Cu and Mo mineralization. The magmatism and mineralization were controlled by the strike-slip fault system that formed after collision of the Lut and Afghan blocks.
- Most mineralization occurs in NW-SE striking quartz veins and veinlets. Minor mineralization also occurs as disseminations, in stockworks, and in breccias. The quartz veins and veinlets that lie within or close to the syenitic to monzonitic stock are typically mineralized, but those further from the stock are barren. This indicates that the Cu-Mo mineralization is genetically related to the syenitic to monzonitic stock.
- The hypogene alteration sequence seen in many porphyry Cu deposits is not well developed at Lar. This is due to the alkaline composition of the host rocks that are enriched in K. The main alteration type is silicic developed along and around fractures, but it is not pervasive. In addition to silicic alteration, potassic and phyllic alteration, with very low pyrite contents, were developed in the mineralized area. Propylitic alteration was formed in the peripheral parts of the mineralized area. Argillic alteration was also locally developed in the mineralized area by supergene processes.
- Generally, the mineralization can be divided into two types, hypogene and supergene. The hypogene mineralization is characterized by chalcopyrite, bornite, molybdenite, and minor pyrite. The supergene mineralization is represented by chalcocite, covellite, malachite, azurite, and iron hydroxides.
- At Lar, a high-grade supergene mineralized zone did not form, probably because the hypogene sulfide contents were low. At Lar, a pyritic crust or pyrite-rich phyllic alteration zone was also absent. Thus, dissolution of the sulfides in the Lar porphyry Cu-Mo deposit

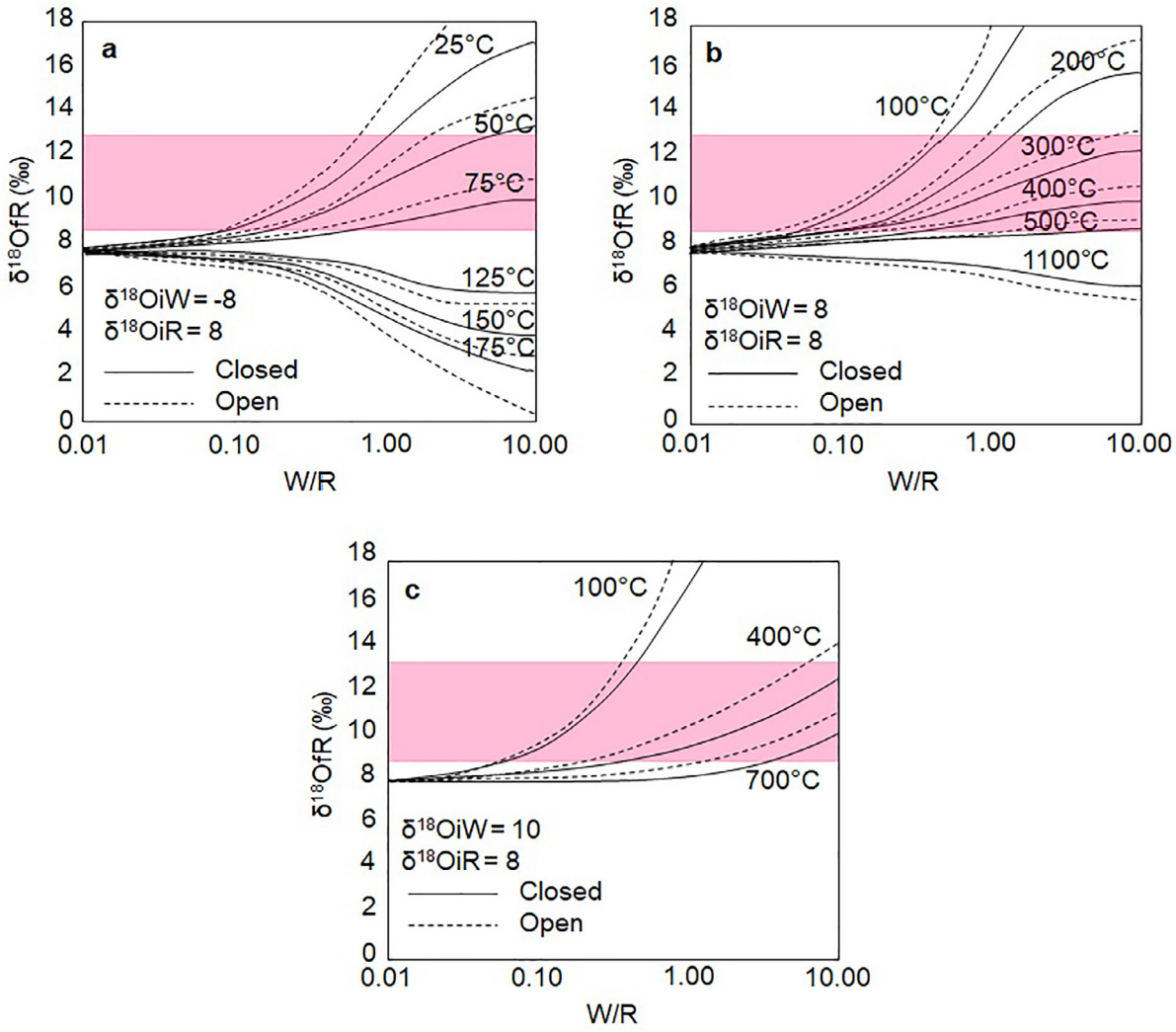

Fig. 24. W/R plots for hydrothermally altered syenites at the Lar porphyry Cu-Mo deposit. Theoretical curves for both open and closed system constrain the W/R ratios were calculated from Taylor (1977) equations. The pink rectangle represents $\delta^{18}O$ in the Lar porphyry Cu-Mo deposit. (For interpretation of the references to color in this figure legend, the reader is referred to the web version of this article.)

by meteoric waters provided insufficient acidic solutions to increase the grade in the supergene zone.

- The narrow range of measured sulfur isotopic compositions for sulfide ore pairs in quartz veins and syenitic intrusions from the study area points to mantle-dominated igneous sources for all hypogene sulfide phases.
- The $\delta^{18}O$ values of the quartz in the veins of silicic and potassic alteration zones vary from 9.57 to 11.51‰. Calculated $\delta^{18}O$ values of H_2O in equilibrium with quartz vary from 6.25 to 10.99‰, falling within the range of magmatic waters, though the higher values could indicate enrichment of $\delta^{18}O$ values of magmatic hydrothermal fluids by interaction with meta-sedimentary rocks.
- Re-Os dating of two molybdenite samples yield ages of 29.72 ± 0.11 and 31.95 ± 0.11 Ma, which provide minimum ages for their hosting intrusions.

Acknowledgements

Mohammad Boomeri, Rahele Moradi, and Sasan Bagheri wrote the paper, and Holly Stein helped with the English. Our thanks to professor David Lentz (University of New Brunswick) who provided feedback on the research and provided valuable comments on the paper. The AIRIE Program kindly provided two molybdenite age for this study. We would like to pass our thanks to the University of Sistan and Baluchestan that provided a part of funding for this research. The authors thank referees of this paper and Jeff Mauk for their valuable comments and suggestions.

References

Bagheri, S., Bakhshi, M.R., 2001. Investigation of north Zahedan magmatism and its relation to ore genesis. Published Research Report. University of Sistan and Baluchestan, Zahedan, Iran.

Barra-Pantoja, L.F., 2005. Applications of the Re-Os isotopic system in the study of mineral deposits: geochronology and source of metals. Ph.D. thesis. University of Arizona.

Berberian, M., King, G.C.P., 1981. Towards a paleogeography and tectonic evolution of Iran. Can. J. Earth Sci. 8, 210–265.

Berger, B.R., Ayuso, R.A., Wynn, J.C., Seal, R.R., 2008. Preliminary model of porphyry copper deposits. Open-File Report 2008–1321. U.S. Department of the Interior, U.S Geological Survey, pp. 55.

Bonin, B., Azzoini-Sekkal, A., Bussy, F., Ferrag, S., 1998. Alkali-calcic and alkaline post-orogenic (PO) granite magmatism: petrological constraints and geodynamic settings. Lithos 45, 45–70.

Booden, M.A., Mauk, J.L., Simpson, M.P., 2011. Quantifying metasomatism in epithermal Au-Ag deposits: a case study from the Waitekauri area, New Zealand. Econ. Geol. 106, 999–1030.

Boomeri, M., 2014. Ore deposits and indexes of Sistan and Baluchestan province. In: 6th Symposium of Iranian Society of Economic Geology.

Boomeri, M., Lashkaripour, G.R., Gorgij, M.N., 2005. F and Cl in biotites from Zahedan granitic rocks. Iranian J. Crystallogr. Mineral. 13, 79–94.

Borthwick, J., Harmon, R.S., 1982. A note regarding ClF3 as an alternative to Br F5 for oxygen isotope analysis. Geochim. Cosmochim. Acta 46, 1665–1668.
Calagari, A.A., 2003. Stable isotope (S, O, H, and C) studies of the phyllic and potassic–phyllic alteration zones of the porphyry copper deposit at Sungun, east Azerbaijan, Iran. J. Asian Earth Sci. 21, 767–780.
Camp, V.E., Griffis, R.J., 1982. Character, genesis and tectonic setting of igneous rocks in the Sistan suture zone, eastern Iran. Lithos 15, 221–239.
Castro, A., Aghazadeh, M., Badrzadeh, Z., Chichorro, M., 2013. Late Eocene-Oligocene post-collisional monzonitic intrusions from the Alborz magmatic belt, NW Iran. An example of monzonite magma generation from a metasomatized mantle source. Lithos 180–181, 109–127.
Chance, P., 1981. Petrogenesis of a low-Ti, potassic suite: Kuh-e Lar caldera subsidence complex, eastern Iran. M.Sc. thesis. University of Western Ontario, London, Ontario, Canada.
Chaussidon, M., Albarède, F., Sheppard, S.M.F., 1987. Sulfur isotope heterogeneity in the mantle from ion microprobe measurements of sulphide inclusions in diamonds. Nature 330, 242–244.
Chengbiao, L., Xingchun, Z., Shouxu, W., Waiquan, W., Chaojian, Q., Kongwen, W., Tao, R., 2008. Sulfur and lead isotope compositions of the Xuejiping porphyry copper deposit in northwest Yunnan, China: tracing for the source of metals. J. Mineral. Petrol. 28, 80–88.
Clayton, R.N., ONeil, J.R., Mayeda, T.K., 1972. Oxygen isotope exchange between quartz and water. J. Geophys. Res. 77, 3057–3067.
Cooke, D.R., Hollings, P., Walshe, J.L., 2005. Giant porphyry deposits: characteristics, distribution, and tectonic controls. Econ. Geol. 100, 801–818.
Cooke, D.R., Hollings, P., Wilkinson, J.J., Tosdal, R.M., 2014. Geochemistry of porphyry deposits. In: Holland, H.D., Turekian, K.K. (Eds.), Second edition Treatise on Geochemistry 13. Elsevier, Oxford, pp. 357–381.
Cox, K.G., Bell, J.D., Pankhrust, R.J., 1979. The interpretation of igneous rocks. George, Allen and Unwin, London, pp. 450p.
Cox, D.P., Singer, D.A., 1988. Distribution of gold in porphyry copper deposits Open-File Report 88-46, U.S. Geological Survey, p. 23.
Deyell, C.L., 2005. Sulfur isotope zonation at the Mt Polley alkalic porphyry Cu-Au deposit, British Columbia, Canada. In: Mao, J., Bierlein, F.P. (Eds.), Mineral deposits research: meeting the global challenge: 8th Biennial Society for Geology Applied to Mineral Deposits Meeting 1, 373–376.
Farhoudi, G., Karig, D.E., 1977. Makran of Iran and Pakistan as an active arc system. J. Geol. 5, 664–668.
Farokh-Nezhad, M., 2011. Geochemical characterization of potassic mafic rocks, monzonites and syenites from Lar complex, eastern Iran. M.Sc. thesis, University of Sistan and Baluchestan, Zahedan, Iran.
Field, C.W., Fifarek, R.H., 1985. Light stable isotopes systematic in the epithermal environment. In: Berger, B.R., Bethke, P.M. (Eds.), Geology and geochemistry of epithermal systems. Reviews in Economic Geology 2, 99–128.
Ghafari-Bijar, S., 2009. Geochemistry of potassic mafic rocks in the Lar complex, north of Zahedan, east of Iran. M.Sc. thesis. University of Sistan and Baluchestan, Zahedan, Iran.
Ghaffar, A., Ghaffar, X.C., Kun, X., Peng, X.Z., Ullah, I., 2016. Geological framework and evolution of the Saindak porphyry Cu-Au deposit, Chagai district, Balochistan, SW Pakistan. Society of Economic Geologists, Inc. SEG-MJD 2016 Conference.
Ghasemi, H., Sadeghian, M., Kord, M., Khanalizadeh, A., 2010. The evolution mechanisms of Zahedan granitoid batholith, southeast Iran. Iranian J. Crystallogr. Mineral. 17, 551–578.
Gustafson, L.B., Hunt, J.P., 1975. The porphyry copper deposit at El Salvador, Chile. Econ. Geol. 70, 857–912.
Hastie, A.R., Kerr, A.C., Pearce, J.A., Mitchell, S.F., 2007. Classification of altered volcanic island arc rocks using immobile trace elements: development of the Th-Co discrimination diagram. J. Petrol. 48, 2341–2357.
Hobbs, B.E.H., Zhang, Y., Ord, A., Zhao, C., 2000. Application of coupled deformation, fluid flow, thermal and chemical modelling to predictive mineral exploration. J. Geochem. Explor. 69–70, 505–509.
Imai, A., 2005. Evolution of hydrothermal system at the Dizon porphyry Cu-Au deposit, Zambales, Philippines. Resour. Geol. 55, 73–90.
Kan Iran Engineering, 1999. Report of the Lar copper deposit geological map. National Iranian Copper Industries Co, Tehran, Iran.
Karimi, A., 2002. Geochemical behaviors and geological studies of copper and paragenesis elements in Lar prospect (north Zahedan). Iranian J. Earth Sci. 43, 56–67.
Kausar, A.B., 1992. Petrology of the Kohistan arc and hosted hydrothermal sulfides, Gilgit area, Pakistan. M.Sc. thesis. Oregon State University, Corvallis, Oregon.
Kirkham, R.V., Sinclair, W.D., 1995. Porphyry copper, gold, molybdenum, tungsten, tin, silver. In: Eckstrand, O.R., Sinclair, W.D., Thorpe, R.I. (Eds.), Geology of Canadian mineral deposit types: Geological Survey of Canada 8, 421–446.
Maanijou, M., Mostaghimi, M., Abdollahy-Riseh, M., Sepahi-Gerow, A.A., 2013. Systematic sulfur stable isotope and fluid inclusion studies on veinlet groups in the Sarcheshmeh porphyry copper deposit: based on new data. Econ. Geol. 4, 217–239.
Madeisky, H.E., 1996. A lithogeochemical and radiometric study of hydrothermal alteration and metal zoning at the Cinola epithermal gold deposit, Queen Charlotte Islands, British Columbia. In: Coyner, A.R., Fahey, P.L. (Eds.), Geology and ore deposits of the American Cordillera 3, 1153–1185.
Markey, R.J., Hannah, J.L., Morgan, J.W., Stein, H.J., 2003. A double spike for osmium analysis of highly radiogenic samples. Chem. Geol. 200, 395–406.
Mauk, J.L., Simpson, M.P., 2007. Geochemistry and stable isotope composition of altered rocks at the Golden Cross epithermal Au-Ag deposit, New Zealand. Econ. Geol. 102, 841–871.
McCandless, T.E., Ruiz, J., 1993. Rhenium-Osmium evidence for regional mineralization in southwestern North America. Science 261, 1282–1286.
McCandless, T.E., Ruiz, J., Campbell, A.R., 1993. Rhenium behavior in molybdenite in hypogene and near-surface environments: Implications for Re-Os geochronometry. Geochim. Cosmochim. Acta 57, 889–905.
Meng, X.J., Hou, Z.Q., Li, Z.Q., 2006. Sulfur and lead isotope compositions of the Qulong porphyry copper deposit, Tibet: implications for the Sources of plutons and metals in the deposit. Acta Geol. Sin. 80, 554–560.
Mohammadi, A., Burg, J.P., Bouilhol, P., Ruh, J., 2016. U-Pb geochronology and geochemistry of Zahedan and Shah Kuh plutons, southeast Iran: implication for closure of the south Sistan suture zone. Lithos 248–251, 293–308.
Moradi, R., 2016. Geochemistry of the Lar Cu and Mo deposit, north of Zahedan. Ph.D. thesis. University of Sistan and Baluchestan.
Moradi, R., Boomeri, M., Bagheri, S., 2014. Petrography and geochemistry of intrusive rocks in the Shurchah antimony-bearing area southeast of Zahedan. J. Petrol. (Isfahan Univ.) 5, 15–32.
Moradi, R., Boomeri, M., Bagheri, S., Nakashima, K., 2016. Mineral chemistry of igneous rocks in the Lar Cu-Mo prospect, southeastern part of Iran: Implications for P, T, and fO2. Turkish J. Earth Sci. 25, 1–16.
Müller, D., Rock, N.M.S., Groves, D.I., 1992. Geochemical discrimination between shoshonitic and potassic volcanic rocks from different tectonic settings: a pilot study. Mineral. Petrol. 46, 259–289.
Nakisa, M., 2002. Summing up exploration of calculating Lar copper ore deposits, Zahedan. Ministry of Industries and Mines, National Iranian Copper Industries Company.
Ohmoto, H., Goldhaber, M.B., 1997. Sulfur and carbon isotopes. In: Barnes, H.L. (Ed.), Geochemistry of hydrothermal ore deposits, 3rd ed. Wiley, New York, pp. 517–611.
Ohmoto, H., Rye, R.O., 1979. Isotopes of sulfur and carbon. In: Barnes, H.L. (Ed.), Geochemistry of hydrothermal ore deposits, 2nd ed. Wiley, New York, pp. 509–567.
O'Neill, J.R., Taylor, H.P., 1969. Oxygen isotope equilibrium between muscovite and water. J. Geophys. Res. 74, 6012–6022.
Ord, A., Hobbs, B.E., Zhang, Y., Broadbent, G.C., Brown, M., Willetts, G., Sorjonen-Ward, P., Walshe, J.L., Zhao, C., 2002. Geodynamic modeling of the century deposit, Mt Isa province, Queensland. Aust. J. Earth Sci. 49, 1011–1039.
Pang, K.N., Chung, S.L., Zarrinkoub, M.H., Khatib, M.M., Mohammadi, S.S., Chiu, H.Y., Chu, C.H., Lee, H.Y., Lo, C.H., 2013. Eocene-Oligocene post-collisional magmatism in the Lut-Sistan region, eastern Iran: magma genesis and tectonic implications. Lithos 180–181, 234–251.
Parsapoor, A., Dilles, J.H., Khalili, M., Mackizadeh, M.A., Maghami, M., 2014. Stable isotope record of hydrothermal sulfate, sulfide and silicate minerals in the Darreh-Zar porphyry copper deposit in Kerman, southeastern Iran: implications for petrogenesis and exploration. J. Geochem. Explor. 143, 103–115.
Pirajno, F., 2010. Intracontinental strike-slip faults, associated magmatism, mineral systems and mantle dynamics: examples from NW China and Altay-Sayan (Siberia). J. Geodyn. 50, 325–346.
Rahnama-Rad, J., Sahebzadeh, B., Mirhajizadeh, A.A., 2008. Weathering and weakness of Zahedan granitoids: A rock engineering point of view. Appl. Geol. 4, 247–257.
Razique, A., 2013. Magmatic evolution and genesis of the giant Reko Diq H14–H15 porphyry copper-gold deposit, district Chagai, Balochistan-Pakistan. Ph.D. thesis. University of British Columbia.
Robb, L., 2005. Introduction to ore-forming processes. Blackwell Publishing, pp. 384.
Sadeghian, M., Bouchez, J.L., Ne de lec, A., Siqueira, R., Valizadeh, M.V., 2005. The granite pluton of Zahedan (southeast of Iran): a petrological and magnetic fabric study of a syntectonic sill emplaced in a transtensional setting. J. Asian Earth Sci. 25, 301–327.
Sadeghian, M., Valizadeh, M.V., 2007. Emplacement mechanism of Zahedan granitoidic pluton with the aid of AMS method. Earth Sci. 17, 126–143.
Seifert, T., 2008. Metallogeny and petrogenesis of lamprophyres in the mid-European Variscides: post-collisional magmatism and its relationship to late-Varsican ore forming processes (Bohemian massif). IOS Press BV, Amsterdam, Netherlands, pp. 1–128.
Serafimovski, T., Tasev, G., Strmić Palinkaš, S., Palinkaš, L.A., Gjorgjiev, L., 2016. Porphyry Cu mineralization related to the small Tertiary volcanic intrusions in the Bučim ore deposit, eastern Macedonia. Geologia Croatica 69, 101–119.
Shafiei, B., Shahabpour, J., 2008. Gold distribution in porphyry copper deposits of Kerman region, southeastern Iran. J. Sci. Islamic Republic Iran 19, 247–260.
Sinclair, W.D., 2007. Porphyry deposits. In: Goodfellow, W.D. (Ed.), Mineral deposits of Canada: A synthesis of major deposit-types, district metallogeny, the evolution of geological provinces, and exploration methods. Geological Association of Canada, St. John's, Newfoundland, pp. 223–243.
Soltaninejad, S., Shafiei, B., 2014. Mineralogical, geochemical and genetic aspects of mineralization in Now-Chun porphyry Mo-Cu deposit, Kerman province, Iran. Scientific Quarterly J. 23, 11–24.
Stanley, C.R., Madeisky, H.E., 1994. Lithogeochemical exploration for hydrothermal ore deposits using Pearce element ratio analysis: Geological Association of Canada Short Course. Notes 11, 193–212.
Stein, H.J., 2014. Dating and tracing the history of ore formation. In: Holland, H.D., Turekian, K.K. (Eds.), Treatise on Geochemistry 13, 87–118.
Stein, H.J., Markey, R.J., Morgan, J.W., Hannah, J.L., Scherstén, A., 2001. The remarkable Re-Os chronometer in molybdenite: how and why it works. Terra Nova 13, 479–486.
Stein, H., Scherstén, A., Hannah, J., Markey, R., 2003. Sub-grain scale decoupling of Re and ^{187}Os and assessment of laser ablation ICP-MS spot dating in molybdenite. Geochim. Cosmochim. Acta 67, 3673–3686.
Stöcklin, J., 1968. Structural history and tectonics of Iran, a review. Am. Assoc. Pet. Geol. Bull. 52, 1229–1258.
Suvorova, V.A., 1974. Temperature dependence of the distribution coefficient of sulfur isotopes between equilibrium sulfides. National Symposium on Stable Isotope

Geochemistry, 5th, Moscow, Program Pt. 1, 128.
Taylor, H.P., 1971. Oxygen evidence for large-scale interaction between meteoric ground waters and tertiary granodiorite intrusions, western Cascade range, Oregon. J. Geophys. Res. 76, 7855–7874.
Taylor, H.P., 1977. Water/rock interactions and the origin of H_2O in granitic batholiths. J. Geol. Soc. London 133, 509–558.
Taylor, H.P., Sheppard, S. M.F., 1986. Igneous rocks: I. Processes of isotopic fractionation and isotope systematics. In: Valley, J.W., Taylor, H.P, O'Neil, J.R. (Eds.), Stable isotopes in high temperature geological processes. Reviews in Mineralogy 16, 227–271.
Tirrul, R., Bell, L.R., Griffis, R.J., Camp, V.E., 1983. The Sistan suture zone of eastern Iran. Geol. Soc. Am. Bull. 94, 134–150.
Turi, B., Taylor, H.P., 1971. An oxygen and hydrogen isotope study of a granodioritic pluton from the southern California batholite. Geochim. Cosmochim. Acta 35, 383–406.
Vaughan, A.P.M., Sacrow, J.M., 2003. K-rich mantle metasomatism control of localization and initiation of lithospheric strike-slip faulting. Terra Nova 15, 163–169.
Vila, T., Sillitoe, R.H., 1991. Gold-rich porphyry systems in the Maricunga belt, northern Chile. Econ. Geol. 86, 1238–1260.
Walker, R., Jackson, J., 2004. Active tectonics and late Cenozoic strain distribution in central and eastern Iran. Tectonics 23, 1–24.
Warren, I., Simmons, S.F., Mauk, J.L., 2007. Whole-rock geochemical techniques for evaluating hydrothermal alteration, mass changes, and compositional gradients associated with epithermal Au-Ag mineralization. Econ. Geol. 102, 923–948.
Zar Azin Gostar Consulting Engineering Company, 2014. Detailed exploration report of the Seyasteragi area. Ministry of Industry, Mine and Trade.
Zhang, Y., Schaubs, P.M., Zhao, C., Ord, A., Hobbs, B.E., Barnicoat, A., 2008. Fault-related dilation, permeability enhancement, fluid flow and mineral precipitation patterns: numerical models. In: Wibberley, C.A., Kurz, W., Imber, J., Holdsworth, R.E., Collettini, C. (Eds.), The internal structure of fault zone: Implications for mechanical and fluid-flow properties. Geological Society, London, Special Publications 299, 239–255.